DESIGN AND EXPERIMENTAL VERIFICATION OF A CLUTCHED PARALLEL ELASTIC ACTUATION MECHANISM FOR LEGGED LOCOMOTION

A THESIS SUBMITTED TO
THE GRADUATE SCHOOL OF NATURAL AND APPLIED SCIENCES
OF
MIDDLE EAST TECHNICAL UNIVERSITY

BY

EMRE TANFENER

IN PARTIAL FULFILLMENT OF THE REQUIREMENTS
FOR
THE DEGREE OF MASTER OF SCIENCE
IN
MECHANICAL ENGINEERING

JANUARY 2022

Approval of the thesis:

DESIGN AND EXPERIMENTAL VERIFICATION OF A CLUTCHED PARALLEL ELASTIC ACTUATION MECHANISM FOR LEGGED LOCOMOTION

submitted by **EMRE TANFENER** in partial fulfillment of the requirements for the degree of **Master of Science in Mechanical Engineering Department, Middle East Technical University** by,

Prof. Dr. Halil Kalıpçılar
Dean, Graduate School of **Natural and Applied Sciences** _____

Prof. Dr. M. A. Sahir Arıkan
Head of Department, **Mechanical Engineering** _____

Assist. Prof. Dr. Ali Emre Turgut
Supervisor, **Mechanical Engineering, METU** _____

Prof. Dr. Uluç Saranlı
Co-supervisor, **Computer Engineering, METU** _____

Examining Committee Members:

Assoc. Prof. Dr. Mehmet Bülent Özer
Mechanical Engineering, METU _____

Assist. Prof. Dr. Ali Emre Turgut
Mechanial Engineering, METU _____

Prof. Dr. Uluç Saranlı
Computer Engineering, METU _____

Assoc. Prof. Dr. Ender Yıldırım
Mechanical Engineering, METU _____

Assist. Prof. Dr. Kutluk Bilge Arıkan
Mechanical Engineering, TED University _____

Date: 14.01.2022

I hereby declare that all information in this document has been obtained and presented in accordance with academic rules and ethical conduct. I also declare that, as required by these rules and conduct, I have fully cited and referenced all material and results that are not original to this work.

Name, Surname: Emre Tanfener

Signature :

ABSTRACT

DESIGN AND EXPERIMENTAL VERIFICATION OF A CLUTCHED PARALLEL ELASTIC ACTUATION MECHANISM FOR LEGGED LOCOMOTION

Tanfener, Emre
M.S., Department of Mechanical Engineering
Supervisor: Assist. Prof. Dr. Ali Emre Turgut
Co-Supervisor: Prof. Dr. Uluç Saranlı

January 2022, 70 pages

This thesis presents modeling and system identification studies of a parallel elastically actuated robotic leg system and then details a clutch mechanism design to increase the overall efficiency of the system. The considered platform is a hopping mechanism constrained in the vertical axis that moves with the help of an electric motor and the integrated tension spring working parallel to the motor. To describe the dynamic motion of the mechanism, including the impact transitions, a linearized mass-spring-damper model and a non-linear model that considers inertial properties of the leg mechanism are considered. A data-driven approach is used to identify the physical parameters of these models. The experimental validation procedure shows the accuracy of the models to predict the motion of the system and implies the linearity of the passive dynamic structure of the mechanism. In addition to the modeling and identification studies, the joint mobility problem of the parallel elastic actuators is addressed. The proposed clutch mechanism intends to bring a compact and reliable solution to this problem while being compatible with the desired dynamic structure of the legged system. A preliminary test setup is used to assess some critical aspects of the clutch.

Also, a modular and compact design is built and integrated on the existing parallel elastic hopper as a proof of concept.

Keywords: legged locomotion, parallel elastic actuation, clutch mechanism, parameter estimation

ÖZ

KAVRAMALI BİR PARALEL ELASTİK EYLEME MEKANİZMASININ BACAKLI HAREKETE YÖNELİK TASARIMI VE DENEYSEL DOĞRULAMASI

Tanfener, Emre
Yüksek Lisans, Makina Mühendisliği Bölümü
Tez Yöneticisi: Dr. Öğr. Üyesi. Ali Emre Turgut
Ortak Tez Yöneticisi: Prof. Dr. Uluç Saranlı

Ocak 2022 , 70 sayfa

Bu tez, paralel elastik eyleyicili bir robotik bacak sisteminin modelleme ve sistem tanılama çalışmalarını sunmaktadır. Ardından sistemin genel verimliliğini artırmak için bir kavrama mekanizması tasarımı detaylandırılmıştır. Ele alınan platform, bir elektrik motoru ve motora paralel çalışan entegre germe yayı yardımıyla hareket eden dikey eksende sınırlandırılmış bir zıplama mekanizmasıdır. Mekanizmanın dinamik hareketini çarpışma mekaniği de dahil edilerek tanımlamak için doğrusallaştırılmış bir kütle-yay-sönümleyici modeli ve bacak mekanizmasının atalet özelliklerini de dikkate alan doğrusal olmayan bir model kullanılmıştır. Bu modellerin fiziksel parametrelerini tanılamak için veri odaklı bir yaklaşım kullanılmıştır. Deneysel doğrulama prosedürü, dinamik modellerin sistemin hareketini tahmin etmekteki başarısını göstermiş ve mekanizmanın pasif dinamik yapısının doğrusallığını ortaya koymuştur. Modelleme ve tanılama çalışmalarına ek olarak paralel elastik eyleyicilerin eklem kısıtlama sorunu ele alınmıştır. Önerilen kavrama mekanizması, bacaklı sistemin istenilen dinamik yapısı ile uyumlu olmakla birlikte bu soruna kompakt ve güvenilir

bir çözüm getirmeyi amaçlamaktadır. Kavrama mekanizmasının bazı kritik yönlerini değerlendirmek için öncül bir test düzeneği kullanılmıştır. Ayrıca, konseptin bir kanıtı olarak mevcut paralel elastik platform üzerine modüler ve kompakt bir tasarım inşa edilmiş ve entegre edilmiştir.

Anahtar Kelimeler: bacaklı robotlar, paralel elastik eyleyiciler, kavrama mekanizmaları, sistem tanılama

ACKNOWLEDGMENTS

I would like to express my sincere gratitude to my supervisor Assist. Prof. Dr. Ali Emre Turgut who has guided and supported me since my undergraduate years. His positive attitude and encouragement kept my motivation alive. I also thank my co-supervisor Prof. Dr. Uluç Saranlı for his support. He introduced the world of legged locomotion to me and gave me a chance to be a part of it.

I am grateful to Assist. Prof. Dr. Mustafa Mert Ankaralı for his tremendous support and guidance towards the end of the study.

This thesis is based on the previous work of Sinan Şahin Candan and Osman Kaan Karagöz. I thank them for their generous help and guidance.

I thank my dear friends and colleagues Batuhan Beşcan, Cem Bilaloğlu, Berk Tosun and Yusuf Can Şimşek, who accompanied me throughout this journey. They were always willing the spare their time whenever I need discussion.

I am grateful to my friends from ATLAS laboratory: Furkan Davulcu, Güner Dilşad Er, Sait Sovukluk and Mert Kaan Yılmaz. They have provided a great work environment and helped me through invaluable discussions.

I would like to express my deepest gratitude to my loving parents Pınar and Adnan Tanfener for their endless support, patience and encouragement. I also thank my brother Tuğrul Tanfener, who has guided me my entire life and kept me motivated with his bitter-sweet criticism, and his lovely wife Gamze Tanfener. Finally, I thank my beloved Büşra Gayretli for her uncoditional love and support.

TABLE OF CONTENTS

LIST OF TABLES

TABLES

LIST OF FIGURES

FIGURES

LIST OF ABBREVIATIONS

2D	2 Dimensional
3D	3 Dimensional
COM	Center of mass
SLIP	Spring loaded inverted pendulum
PEA	Parallel elastic actuation
SEA	Series elastic actuation
NMSE	Normalized mean square error
MAE	Mean average error
OPS	Orthoplanar spring

CHAPTER 1

INTRODUCTION

1.1 Motivation and Problem Definition

Evident from nature itself, legged locomotion promises a significant advantage over other mobile platforms in unstructured terrain. Therefore, over the last few decades, there has been extensive research to understand the underlying dynamics behind the legged animals and apply those principles in mobile robotic platforms. Highly efficient dynamic legged locomotion in nature is associated with the compliant structure of the animals. By its very nature, legged locomotion includes continuous impactive footsteps, and animals have to preserve their energy through those impacts. Recent legged robots show great athletic capabilities by utilizing the same compliant actuation principle. "Spring Loaded Inverted Pendulum" (SLIP) model is proven to capture the center of mass (COM) dynamics of the running animals. This model claims that although the animals are composed of a complex bio-mechanical system, overall motion can be modeled as a point mass bouncing on a springy leg. Whereas some research groups try to enforce their system to mimic the dynamics of this model, others benefit from the stable nature of this compliant behaviour in the joint control level and apply closed loop control algorithms to obtain a stable dynamic motion. To have a realization of these model-based controllers in robotic platforms, physical architecture and actuation sub-system of the hardware should be suitable for the model considered by the controller.

There are two main emerging approaches to obtain compliant behavior in robots in terms of hardware architecture. The first approach uses high torque capacity backdrivable actuator units to apply impedance control for the desired motion. Backdriv-

ability implies the low friction and inertia of the actuator unit and plays a crucial role in reducing the losses. These robots possess mechanical simplicity since direct drive actuators are mostly used with relatively simple transmission mechanisms. Also, they provide very high control bandwidth. On the other hand, relying on the actuators even for standing up, robot consumes a significant amount of energy.

The other method is the integration of elastic elements into the hardware to capture the desired dynamics passively. Passive elastically actuated systems are classified by the configuration of the passive compliant element relative to the active actuator. Series and parallel elastic actuation are the two standard configurations. Many robotic platforms successfully utilize series elastic actuation (SEA). It is favorable because the compliant element prevents the actuator from direct impactive loads. This way, one can use actuators with higher reduction ratios to meet the high torque requirements in legged systems. However, the actuator should be powerful enough to deform the series elastic element, and the bandwidth of the elastic element restricts its actuation frequency. Parallel elastic actuation (PEA) provide high energy efficiency as the parallel elastic element provides a significant amount of the required torque additive to the actuator. Therefore, it helps to reduce the required peak torques of the actuator and enables one to use relatively small actuation units. Also, since both the actuator and the passive element create additive forces/torques at the endpoint, the actuator can provide a higher control bandwidth. Despite its efficiency, not too many robots benefit from parallel elasticity. Although it is helpful to store and release energy repeatedly in cyclic motion tasks, when the joints have to increase motion range, such as making a maneuver to avoid obstacles, parallel elastic element opposes the actuator. To overcome this drawback, a solution for adjusting or eliminating the parallel elastic element during the unwanted stages of locomotion is required.

This thesis considers a parallel elastically actuated hopping leg mechanism that is constrained to move only in the vertical axis. The mechanism is designed by Candan et al. [1]. Its novel aspect is integrating a wrapping cam mechanism that results in an equivalent linear spring in the hopping direction. This mechanism aims to have a structure with very similar dynamics to the one described by the SLIP controller. So that, it will be a robotic platform to realize and test controllers based on the abstract SLIP model. In the context of this study, detailed modeling of the described mech-

anism is provided. Then, dynamic hopping experiments on the built setup are used to evaluate the accuracy of the models to predict the trajectory of the motion. Also, the linearity of the system is verified. Even though the models present the system's dynamics as intended, joint restriction problems remain unsolved for the application of this leg on a complete robotic platform. For that purpose, a clutch mechanism is designed. The crucial features of the clutch are its compactness, reproducibility, and suitability for the desired controllers.

1.2 The Outline of the Thesis

Chapter 3 introduces the considered hopping leg mechanism. Firstly, operating principle and the kinematics of the system are explained. Then, mathematical models used to describe the dynamics of the mechanism are detailed and example simulations are presented.

Chapter 4 details the experimental platform. Firstly, components of the physical setup are introduced. Then, control of the system to obtain the desired jumping motion is explained. The function of each component affecting the overall motion and limitations of the system are detailed. Lastly, parameter estimation studies for obtaining the physical properties of the components that affect the dynamics introduced in Chapter 3 are reported. Estimated parameters are tested in a systematic validation process.

Chapter 5 aims to bring a solution to the practical disadvantage of the PEA. A clutch mechanism is proposed for the elimination of the joint restriction problem. The proposed mechanism is explained in detail, and preliminary tests that underline the essential aspects of the mechanism are shown. Lastly, a modular design integrated into the existing hopping mechanism is shown.

CHAPTER 2

LITERATURE SURVEY

After the ground-breaking success of the legged robots of Raibert [2], efforts to describe energy efficient legged locomotion are accelerated. Spring loaded inverted pendulum model (SLIP) is reported to capture the basic dynamical properties of the legged animals by representing the overall system as a point mass bouncing on springy legs [3, 4]. Although this model is a reduced representation of the complex mechanical systems, it still does not have an analytical solution for the planar bouncing motion. However, in [5], it is shown that the approximate analytical solution is possible to predict the motion of the model. Some researchers utilize the compliant behavior not for analytically predicting and controlling the motion but only to benefit from its stable nature by implementing it in the joint level [6, 7, 8].

Controlling a robot to adopt the dynamics of a simpler model like SLIP is beneficial; however, it is not easy as real robots have complex mechanical structures. The robot's mechanics should be designed to be suitable for the target model to some extent, and further control actions are required. Moreover, accurate information about the dynamical parameters of the system should be known. Khalil and Dombre [9] underlines the difficulty of direct measurements to obtain precise inertial parameters. They propose the identification method based on the analysis of input-output measurements of a system to form an overdetermined least-squares formulation. Gautier [10] applies this approach on the power level of the dynamical model to filter out the noisy acceleration measurements. Uyanık et al. [11] estimates the dynamical parameters of a spring-loaded monopedal robot by using the approximate analytical solution of the target SLIP model and evaluates its predictive performance. Key features of the leg design for realizing spring like running controllers are provided in [12]. In [13],

operational space control method is employed to realize SLIP model in a articulated robotic leg. Poulakakis and Grizzle use the hybrid zero dynamics method to realize the SLIP model on a massless leg integrated with body dynamics.

Robots utilizing compliant actuation strategy can be divided into two main groups. The first group of robots presents active compliance by the impedance control of the actuators. MIT Cheetah family robots are one of the first to present highly dynamic and efficient legged locomotion with direct drive electric motors [14]. They also formalize the actuator morphology with low reduction ratios and lightweight leg structure to minimize impact losses and eliminate the non-linear inertial effects. This actuation structure provides mechanical simplicity with a reasonably simple transmission structure. With the increasing availability of high-performance BLDC motors, the number of dynamic robots has dramatically increased in the last decade. MIT mini cheetah quadruped [15] robot proved that this actuation design could use off-the-shelf components to obtain competitive dynamic behaviors. The robot is reported to be the only quadruped that can perform back-flip. Minitaur [16], Stanford Doggo [17], SOLO [18] are the other example robots that have the similar actuation principle.

The other design approach is based on the passive dynamics of the system with the integration of elastic components like springs. This approach is called passive because the mechanical structure of the system provides compliance without any actuation. The history of this kind of robot dates older than the first group as utilizing a spring is mainly preferred to use traditional electric motors with a large gearbox. The elastic component placed in the drive-train helps restore the system's energy, which otherwise would be lost due to the high inertia and friction of the large reduction ratios of the gearbox. Raibert's robots that utilize air springs in conjunction with the high force hydraulic actuators serve as one of the earliest examples of passive dynamic locomotion. Passive compliance is commonly implemented through the series elastic actuation (SEA), where spring is placed between the actuator and the end-effector. Quadruped robot Starleth [19] and its continuation Anymal [20], biped robot ATRIAS [21] are the successful examples that employ series elastic elements to achieve dynamic locomotion. As the elongation of the spring placed between the actuator and the ground introduces a new degree of freedom to be controlled, auxiliary sensory

equipment to measure spring deflection and relatively complex control strategies to compensate for the extra degree of freedom is common to those platforms. A feedback linearization method is presented in [22] to apply SLIP model in a more complex SEA monopedal robotic platform.

The other configuration uses the compliant element in parallel to the actuator that actively works. In this configuration, energy provided to the system directly adds up to the energy input of the actuator. Therefore, parallel elastic element tends to reduce the load on the actuator. Yesilevskiy et al. [23] evaluate and compare the effectiveness of both SEA and PEA for hopping motion, with both of them having the most optimal parameter configuration. With a simulation-based study, they imply the superiority of the PEA when the presence of high frictional losses of the transmission of the SEA. However, they underline that even if PEA configuration reduces the peak torque requirement and thus the thermal losses, SEA is superiror in terms of the overall positive motor work. ERNIE biped robot [24] incorporate extension springs working parallel to the knee actuator. It is reported to increase overall efficiency for cyclic walking motion on a trade mill. ERNIE is claimed to achieve stable dynamic walking trajectories. Spacebok robot developed in ETH [25], uses parallel springs in its parallel leg mechanism. It benefits from the high output forces from the parallel spring to reach high jumping heights. The platform is intended to be used in rough environments like the surface of the planets, where it should overcome enormous obstacles.

Although it is evident that the parallel elastic elements reduce the torque/force requirement and increase efficiency, they are rarely used in legged robots. In cyclic running or hopping locomotion , parallel elastic component stores the energy during the stance phase and helps the actuator exert forces. However, it is expected that the robot may change its periodic trajectory by increasing ground clearance of the leg to avoid obstacles in uneven terrain. Also, most of the time, robots use their legs for numerous manipulative tasks in addition to running or hopping. In these instances, parallel elasticity limits the joint motion and reduces overall efficiency [26]. So, a complementary solution for eliminating the joint restriction is needed. Otherwise, implementation of PEA would be constrained to the restricted applications as seen in the [24] and [25].

The apparent attempt is to somehow engage and disengage the compliant element in different phases of the gait to eliminate it when it is not required. Haufle et al. [27] introduces a bench-top parallel elastic actuator with a clutch mechanism that uses an electromagnetic brake to eliminate the parallel spring when it is not required. The case scenario they consider is the bouncing motion of a legged system where the system tries to stop itself. Since the parallel elastic element forces the system to continue hopping, it has a negative effect against the actuator that tries to stop the motion. The system is represented with the bench-top actuator, and the clutch's effect to remove the spring's negative effect is evaluated. They report up to 66% reduction in peak torque requirement and 80% in overall energy requirement. However, the mechanism is reported to produce unwanted vibratory distortion in the disengagement instant, and the mechanism struggled to preserve accuracy in an unexpected touch-down scenario. Diller et al. [28] details the design of a lightweight electroadhesive clutch for ankle exoskeleton device. The working principle is based on the electrostatic adhesion between large electrode sheets. While the mechanism provides large forces relative to its mass, the study focuses on the actuator design. [29] proposes a design for a clutched parallel elastic actuator for the hip joint of an exoskeleton device. Discrete end positions are created for the parallel spring to be attached. With the aid of an auxiliary actuator, the mechanism changes the end position of the parallel spring to a different location and changes its effective stiffness. SPEAR monopedal robot [30] presents a modular application of a switch mechanism to change the parallel compliance. It utilizes an auxiliary soft spring attached in series to the parallel spring. Having a soft spring in series, the equivalent stiffness of the springs reduces significantly, and the leg can move freely. When the leg of the robot steps on the ground, it passively fixes the point in between the two springs and activates the parallel spring. It is one of the few implementations of such a switch mechanism on a mobile robotic platform and benefits from the simplicity of the engagement action without any extra actuators. It uses a key and a chain couple to fix the spring, and this configuration is reported to cause sticking time to time during disengagement.

2.1 Contributions

The platform built by Candan et al. [1] aims to prove that passive dynamic structure obtained by wrapping cams creates a target platform for the SLIP model. The most critical aspect of the design is whether the wrapping cam results in a linear spring force in the desired axis. Because if such a mechanism functions properly, one can realize SLIP-based controllers on this platform while benefiting from the energetic advantage of the passive compliant element. In [1], mechanism is validated with static force measurements. This study extends the static measurements to dynamic hopping experiments to show that the mechanism preserves a linear passive dynamic structure as described in the SLIP model.

The development of an efficient complementary solution for the joint mobility problem of the parallel elastic actuators in mobile-legged robots remains unsolved. This study proposes a novel clutch mechanism. The working principle of the proposed design takes it inspiration from the SPEAR robot [30]. However, in contrast to the SPEAR, the mechanism is designed to be compactly located on the robot's body to preserve the lightweight leg structure, making it convenient for the SLIP model. Also, components are designed to be 3D printed whenever possible, and off-the-self components are used to reduce the overall weight and increase reproducibility. A prototype of the mechanism is produced, and preliminary tests are conducted for proof of concept.

CHAPTER 3

METHODS

This chapter deals with the mathematical modeling of the considered leg mechanism. Firstly, the overall structure of the system will be introduced, and then the dynamic models that capture the motion of this structure will be examined in detail.

3.1 Description of the System

Considered system is given in the Figure 3.1. It is a 5 link mechanism with passive compliance. The mechanism is constrained to move only vertically with the prismatic joints at the body and the toe. All links are interconnected with revolute joints.

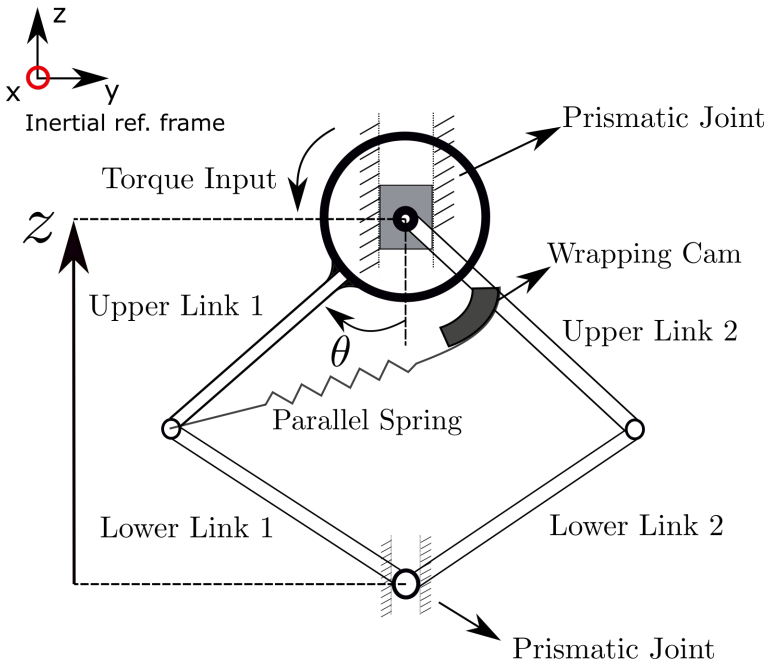

Figure 3.1: Description of the mechanism.

Only one actuator is placed on the body to apply torque input between two upper links. The compliant element is a tension spring that stores energy while the leg shortens in the radial direction. As the upper links rotate relatively, the spring is being wrapped on the surface of a cam. This wrapping cam is designed to have a surface that maps the elongation in the spring to a linear virtual elongation in the radial axis of the leg [1]. So, the system is assumed to have an equivalent virtual spring between the body and the leg, as depicted in Figure 3.2. The system is parallel elastically actuated considering the generated force at the end effector (toe). Because forces created on the toe by the actuator torque input and the equivalent virtual spring directly add up. The primary function of the mechanism is to realize hopping motion in the vertical axis with the aid of the torque input and the parallel spring. The nature of hopping motion leads to a continuous change of the interaction between the leg and the ground. Therefore, the motion of the leg can be examined in different phases:

- The leg is said to be in the stance phase as the toe remains in contact with the ground and the leg can apply force against it to change its momentum.
- The leg is said to be in the flight phase as the toe loses contact with the ground and the leg cannot change its momentum.

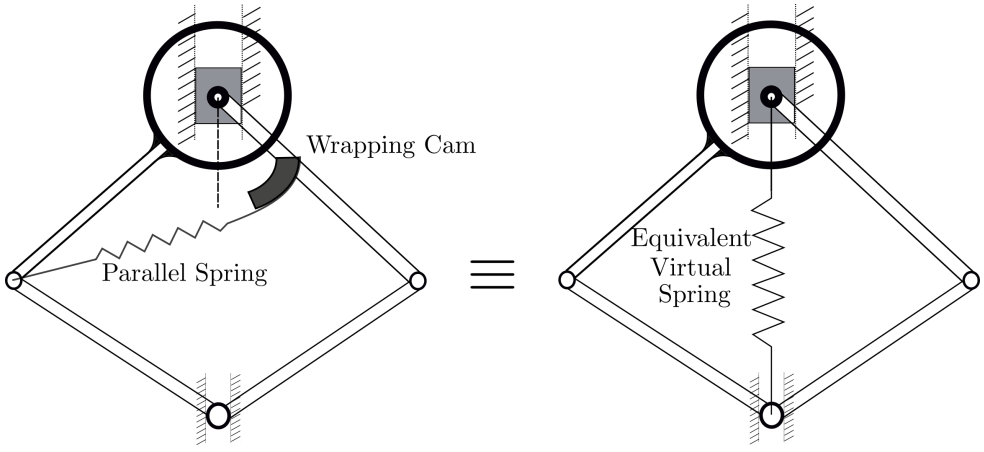

Figure 3.2: Mapping of the parallel spring

All links have an equal leg length L, and the leg angle, θ, changes between $20^\circ - 60^\circ$. Assuming that there is a mechanic stopper, at $\theta = 20^\circ$ mechanism starts to jump. As the mechanism in the stance phase, assuming that the toe does not slip and remains

still, the relation between the COM height z and the leg angle θ can be described as:

$$z_c = z - 2Lcos(\theta) \tag{3.1}$$

Where, z_c is the vertical position of the contact point.

3.2 Dynamical Models

This section deals with the derivation of mathematical models that describe the hopping motion of the leg mechanism. As explained in the previous section, the leg experiences different phases during the locomotion cycle. So, a single set of equations is not sufficient to capture the system's behavior for all of the locomotion cycle. This situation is called hybrid dynamics, which means that the dynamics of the system change in different phases. Therefore, one must consider the dynamics of different phases separately while also considering the phase transitions.

Two models are considered in this study: the first is a reduced model that is composed of a point mass bouncing on a linear spring-damper couple. The second is a non-linear model that also accounts for the leg structure's inertial parameters. The first model is favorable for control purposes since the linear mass-spring-damper model has analytical solutions. On the other hand, the non-linear model captures a more realistic case considering inertial parameters and impact collisions. In the following sections, models will be introduced in further detail.

3.2.1 Linear Model

In a generic articulated leg structure, inertial properties of the links result in a non-linear equation of motion, including Coriolis and gravitational terms. The linearized model neglects these inertial effects to obtain a simpler linear model with analytical solutions. Figure 3.3 illustrates the linearized model. m is the point mass lumped at the body. k is the equivalent spring constant. F_{in} is the force created at the toe by the motor torque during the stance phase. Frictional losses are modeled as linear viscous damping proportional to the velocity in the vertical direction. d_s and d_f are the viscous damping coefficients in the stance and flight phases, respectively. Note

that the system experiences a free-fall motion without any actuation and spring force during the flight phase. However, since the system is still attached to the linear guide, frictional loss exists.

Motor torque should be converted to the vertical force as the model moves in the vertical axis. During the stance phase toe is assumed to be pinned to the ground. The force created by the actuator at the toe can be found by using the previously introduced kinematics relation 3.1. From the virtual work equivalence:

$$\tau\delta\theta = F\delta z \tag{3.2}$$

$\delta\theta$ and δz are the infinitesimal displacements in the leg angle and vertical axis, respectively. Relation between the infinitesimal change in position variables can be obtained using the 3.1:

$$\delta z = 2Lsin(\theta)\delta\theta \tag{3.3}$$

One can isolate $\delta\theta$ from 3.3 and put into 3.2 to obtain the input force created by the motor.

$$F_{in} = \frac{\tau}{2Lsin(\theta)} \tag{3.4}$$

Where, τ is the motor torque and L is the fixed link length.

Two state variables that define the motion of the system are the vertical position and velocity of the point mass, z and $\dot{z}$, respectively. z_0 is the position where the spring has the rest length.

Equation of motion of the system in the stance phase is described by:

$$m\ddot{z} + k(z - z_0) + d_s\dot{z} + mg = F_{in} \tag{3.5}$$

Equation of motion of the system in the flight phase is described by:

$$m\ddot{z} + d_f\dot{z} + mg = 0 \tag{3.6}$$

3.5 and 3.6 can be written in state space form:

$$\dot{\mathbf{x}} = A\mathbf{x} + B\mathbf{u} \tag{3.7}$$

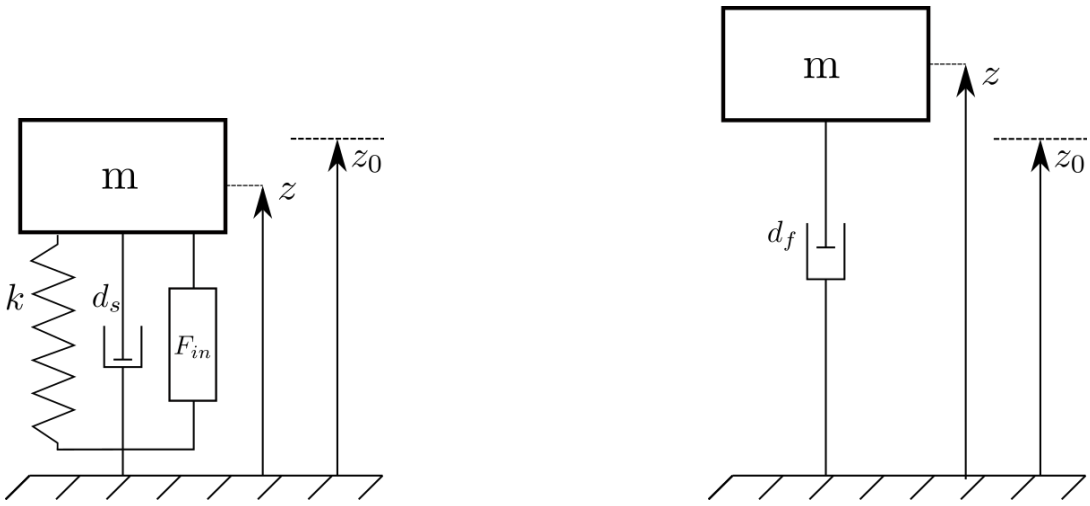

(a) Stance Phase

(b) Flight phase

Figure 3.3: Dynamic model of the linear system

Where,

$$\mathbf{x} = \begin{bmatrix} z(t) \\ \dot{z}(t) \end{bmatrix}$$

$$A = \begin{cases} \begin{bmatrix} 0 & 1 \\ -\frac{k}{m} & -\frac{d_s}{m} \end{bmatrix} & \text{, if stance phase} \\ \\ \begin{bmatrix} 0 & 1 \\ 0 & -\frac{d_f}{m} \end{bmatrix} & \text{, if flight phase} \end{cases}$$

$$B = \begin{bmatrix} 0 \\ \frac{1}{m} \end{bmatrix}$$

$$\mathbf{u} = \begin{cases} kz_0 - mg - F_{in}(t) & \text{, if stance phase} \\ -mg & \text{, if flight phase} \end{cases}$$

Although this structure has analytical solutions for given initial conditions $z(0)$ and

$\dot{z}(0)$ in continuous time, converting this state space form into discrete-time is favorable. Working in the discrete-time state space model is suitable for simulation purposes, and choosing a proper, fixed sampling rate makes it easily comparable with the experimental results. Discretizing the model with a zero order hold at a $1khz$ sampling frequency, solution of the model becomes:

$$x[n+1] = A_d x[n] + B_d u[n] \tag{3.8}$$

Where, A_d and B_d are the discretized state and input matrices with the fixed sampling rate. Equation 3.8 can easily be solved with the given initial conditions $x(0) = [z(0), \dot{z}(0)]^T$ by using a sequential loop in a programming environment like MATLAB.

State Transitions and Impact

Having described the equation of motion for stance and flight phases separately, what is missing for a complete mathematical expression of the hopping is the transition between the two states:

$$\dot{z}_{td}^{+} = \alpha_{td} \dot{z}_{td}^{-} \tag{3.9}$$

$$\dot{z}_{lo}^{+} = \alpha_{lo} \dot{z}_{lo}^{-} \tag{3.10}$$

The term α is a parametric expression of the abrupt velocity change at the phase transitions. Subscripts td and lo refer to the touch-down and lift-off instants, respectively. We assume that flight to stance transition occurs when the COM position becomes equal to the free length of the leg, $z = 2Lcos(20^\circ)$. Stance to fight transition occurs when the ground reaction force becomes zero, $F_{GRF} = 0$, or the COM position becomes equal to the free length as in the flight to stance transition.

An example simulation of the model using the 3.8 can be seen in the Figure 3.4. Initial conditions are given as $z(0) = 0.35m$, $\dot{z}(0) = 0m/s$. And selected system

parameters are

$$L = 0.15m$$
$$k = 600N/m$$
$$m = 1.5kg$$
$$d_s = 5Ns/m$$
$$d_f = 1Ns/m$$
$$\alpha_{td} = 1$$
$$\alpha_{lo} = 1$$

System is actuated with a harmonic torque input.

$$\tau = Tsin(\frac{t}{P}2\pi)$$

Where the amplitude $T = 2Nm$, period $P = 0.3s$. Vertical input force seen in the Figure 3.4c is obtained by:

$$F_{in} = \frac{\tau}{2lsin(\theta)}$$

This input profile is chosen to excite the system close to its natural frequency so that uninterrupted hopping motion can be obtained.

Same simulation is repeated with the updated impact parameters $\alpha_{td} = 0.8$ and $\alpha_{lo} = 0.9$. One can see the discontinuous jump effect of the impact on the linear velocity in Figure 3.5

3.2.2 Non-linear Model

In contrast to the linear model, the inertial properties of the leg links are not neglected in this model. All link lengths are assumed to be known perfectly, and all four links are equal in length. However, the center of mass of the links is unknown and left as parametric. The inertia of the links is defined about the center of mass of each link. Body of the system is constrained in the vertical direction. This constraint would be satisfied with a linear guide element in the real mechanism. Thus, a guide element whose mass contributes to the dynamics is considered a separate mechanism link. Equation of motion is obtained by using the Lagrangian method. One can separate

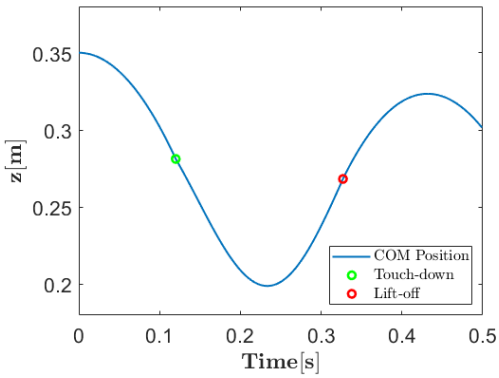

(a) Trajectory of the COM position

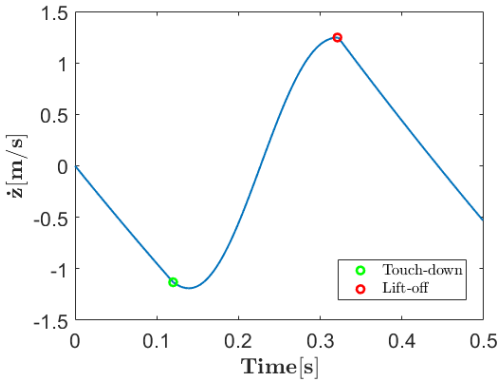

(b) Trajectory of the COM velocity

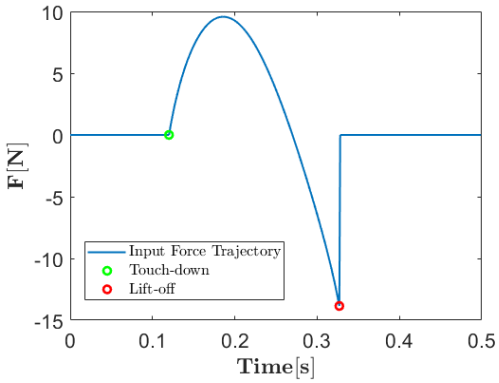

(c) Trajectory of the input force

Figure 3.4: Example simulation of the linear model

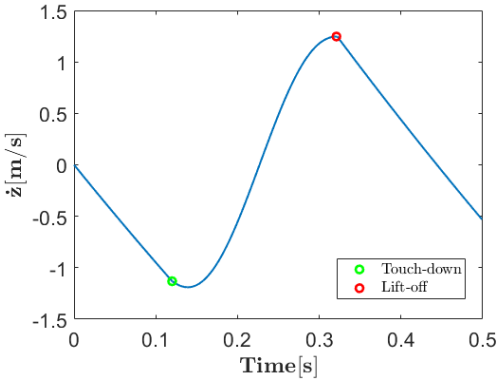

(a) $\alpha_{td} = 1$, $\alpha_{lo} = 1$

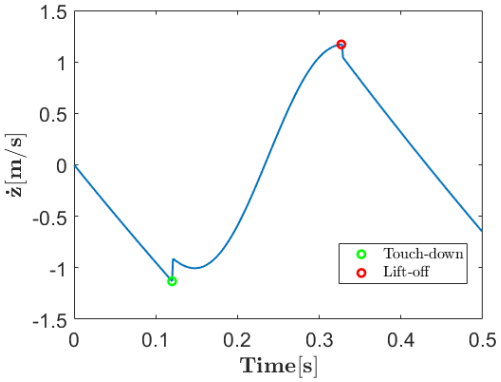

(b) $\alpha_{td} = 0.8$, $\alpha_{lo} = 0.9$

Figure 3.5: Effect of different impact parameters on the COM velocity

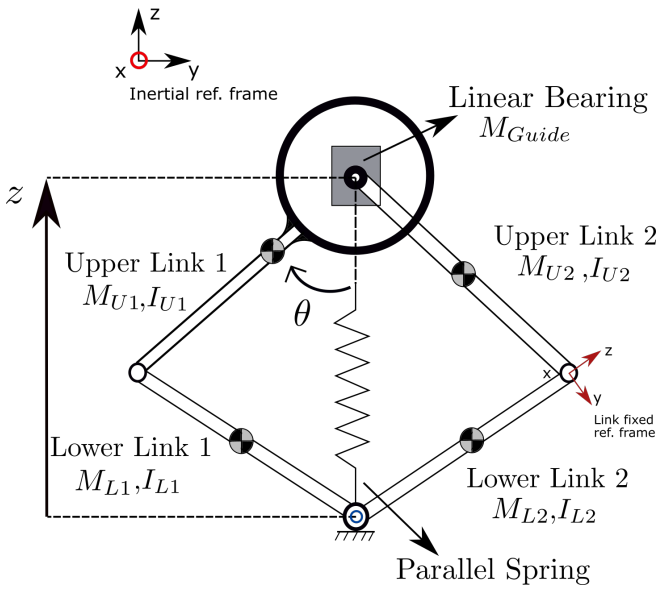

Figure 3.6: Non-linear model

the stance and flight phases as in the linear model and solve the dynamics of both phases with the phase transitions. However, a more compact formulation would be writing down a single unified equation of motion with the contact constraints. This formulation is a variation of the constrained the Lagrangian dynamics. In the general form, the equation of motion of the second order mechanical system is described as:

$$M(q)\ddot{q} + B(q,\dot{q}) + G(q) = J_c^T F_{ext} + \tau \tag{3.11}$$

Where $q = \begin{bmatrix} z & \theta \end{bmatrix}^T$ is the vector of generalized coordinates. $M(q)$ is the mass matrix, $B(q,\dot{q})$ is the coriolis matrix, $G(q)$ is the matrix of gravitational terms. J_c^T is the contact Jacobian of the toe point with respect to the inertial reference frame. It maps the external ground reaction forces acting on the toe to the generalized coordinates, so that all of the terms in the equation of motion are consistently expressed in the same coordinate domain. Finally, τ is the input torque vector. For this specific mechanism, $\tau = \begin{bmatrix} 0 & \tau_{motor} \end{bmatrix}^T$ since the motor located at the body do work only on the leg angle coordinate.

Usually, in the classical Lagrange formulation, contact and internal joint forces that do not actively work on the system are not considered. As in the linear model, toe point is assumed to be pinned to the ground and its position does not change in the stance phase. Therefore, there is a relation between the leg angle θ and the COM position z

leading to a single degree of freedom. However, in the constraint consistent dynamics (or constraint Lagrange formulation), we treat the system as if both the leg angle and the COM position can change at any time. So, the equation of motion will be obtained with two degrees of freedom. Then the contact constraint will be introduced to have a consistent dynamic formulation, also providing the ground reaction forces. Procedure followed to obtain the equation of motion is summarized below:

- For each link, a body fixed reference frame is attached on top of that link and transformation matrices with respect to the inertial frame are obtained.
- Having transformation matrices, COM of each link is written down as parametric w.r.t the inertial reference frame. Here, position of the COM is taken as an unknown parameter located on the z axis of the body fixed frame.
- Link velocity of each link is obtained by differentiating the COM position with respect to the time.
- Angular velocity of each link is computed by using transformation matrix

  $$\tilde{\omega} = \hat{C}^{(I,b)T}\dot{\hat{C}}^{(I,b)}$$

  Where the transformation matrix, $\hat{C}^{(I,b)}$, is between body frame and the Inertial frame.
- Compute the total translational kinetic energy:

  $$T_{tr} = \sum_{i=1} \frac{1}{2} m_i \dot{r}_i^T \dot{r}_i$$

- Compute total rotational kinetic energy:

  $$T_{rot} = \sum_{i=1} \frac{1}{2} \omega_i^T I_i \omega_i$$

  Where the I_i is the inertia of the i^{th} link defined about its COM.
- Compute total potential energy with gravitational potential of each link and the elastic potential energy of the spring:

  $$V = \sum_{i=1} m_i g r_z + \frac{1}{2} k (z - z_0)^2$$

- Define the viscous dissipation power:

$$D = \frac{1}{2} d\dot{z}^2$$

  Where, the d is damping coefficient.

- After that Lagrangian can be formed using total kinetic and potential energy terms and equation of motion can be obtained

$$L = T - V$$
$$\frac{d}{dt}\frac{\partial L}{\partial \dot{q}} - \frac{\partial L}{\partial q} + \frac{\partial D}{\partial \dot{q}} = \lambda$$

  Where, λ is the external forces that actively do work on a generalized coordinate.

Following the summarized procedure, unknown terms of 3.11 can be obtained as follows:

$$M(q) = \begin{bmatrix} a - cos(2\theta)2Lb & sin(\theta)e \\ sin(\theta)e & m_{total} \end{bmatrix} \tag{3.12}$$

$$B(q, \dot{q}) = \begin{bmatrix} sin(2\theta)2L\dot{\theta}^2 \\ cos(\theta)e\dot{\theta}^2 + d \end{bmatrix} \tag{3.13}$$

$$G(q) = \begin{bmatrix} sin(\theta)ge + 2kL^2(cos(\theta) - cos(\theta_0))^2 \\ gm_{total} \end{bmatrix} \tag{3.14}$$

Where,

$$a = I_{U1} + I_{U2} + I_{U1} + I_{L2} +$$
$$m_{L1}(r^2_{COML1} + L^2) + m_{L2}(r^2_{COML2} + L^2) + m_{U1}r^2_{COMU1} + m_{U2}r^2_{COMU2}$$
$$b = m_{L1}r_{COML1} + m_{L2}r_{COML2}$$
$$e = m_{L1}(r_{COML1} + L) + m_{L2}(r_{COML2} + L) + m_{U1}r_{COMU1} + m_{U2}r_{COMU2}$$
$$m_{total} = m_{L1} + m_{L2} + m_{U1} + m_{U2} + m_{Guide}$$

In above, k is equivalent spring coefficient, L is the link length equal for each link. Subscripts U and L denote "Upper link" and "Lower link", respectively. r_{COM} is the distance to the COM of a link from the body fixed reference frame of the same link in the z axis.

Ground reaction force appearing in equation 3.11 can be solved using the contact constraint. That is simply defined as contact point remains still without changing its position. Toe point can be described in terms of generalized coordinates using the contact Jacobian. Contact Jacobian transforms change in the generalized coordinates to change in a given point:

$$\dot{r}_c = J_c \dot{q}$$

For the vertically hopping system, considering only the z coordinate, J_c can be defined as:

$$J_c = \begin{bmatrix} \frac{\partial r_c}{\partial \theta} & \frac{\partial r_c}{\partial z} \end{bmatrix}$$

Using the kinematics of the contact point given in 3.1:

$$J_c = \begin{bmatrix} 2Lsin(\theta) & 1 \end{bmatrix}$$

Then, contact constraint can be described with J_c:

$$r_c = constant \tag{3.15}$$

$$\dot{r}_c = 0 \Longrightarrow J_c \dot{q} = 0 \tag{3.16}$$

$$\ddot{r}_c = 0 \Longrightarrow \dot{J}_c \dot{q} + J_c \ddot{q} = 0 \tag{3.17}$$

Equation 3.17 can be inserted back to 3.11 to solve the ground reaction force.

$$F_c = (J_c M^{-1} J_c^T)^{-1} (J_c M^{-1} (\tau - B - G) + \dot{J}_c \dot{q}) \tag{3.18}$$

Non-linear terms of the equation of motion do not allow to solve it analytically without a linearization. Therefore, numerical simulations are used to obtain the resulting motion trajectory. MATLAB's non-stiff ordinary differential equation solver ODE45 is used to integrate the dynamics with the given input. ODE45 incorporates events so that the solver is able to change dynamics in between different phases. A sample single stride simulation is run and compared with the linear model. Parameter set for both models are presented in Table 3.1. Inertial parameters a, b and e are computed assuming that the lower links have $50gr$ and upper links have $500gr$ and $300gr$ of mass. $10^{-4}kgm^2$ inertia for lower links and $9\ 10^{-4}kgm^2$ for upper links is defined around theri COM. All link lengths are taken as equal and $0.15m$. Resulting COM position and velocity trajectories for both model is presented in Figure 3.7.

Model	m	k	d_s	d_f	a	b	e	α_{td}	α_{lo}
	[kg]	[N/m]	[Ns/m]	[Ns/m]	[kgm^2]	[kgm]	[kgm]	[-]	[-]
Linear	1.6	600	5	1	-	-	-	0.9	1
Non-Linear	1.6	600	5	1	42 10^{-4}	75 10^{-4}	38 10^{-3}	-	1

Table 3.1: Simulation parameters for two different models

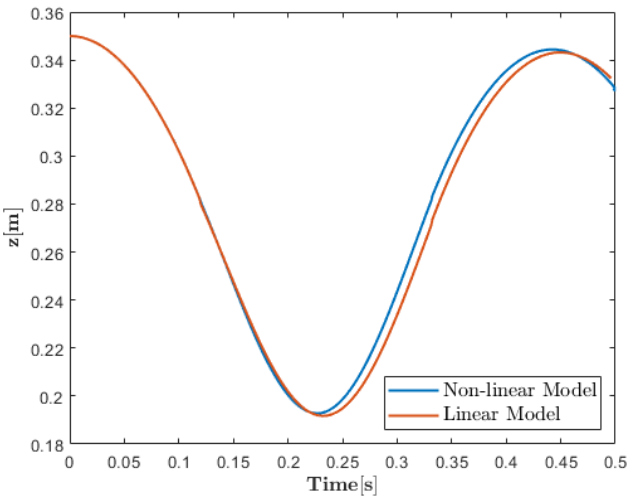

(a) Comparison of the COM position

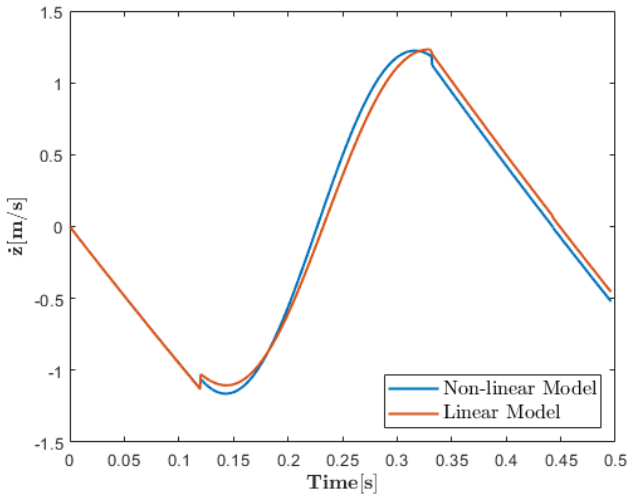

(b) Comparison of the COM velocity

Figure 3.7: Example single stride simulation for comparing linear and non-linear models

CHAPTER 4

EXPERIMENTAL PLATFORM

An experimental setup is built by Candan et.al [1] to realize the hopper mechanism described in Figure 3.1. They have used static force measurements to show that wrapping cam mechanism seen in the Figure 4.1b converts elongation of the parallel spring to a virtual linear spring force in the radial axis. The same setup is used in this study and the static force measurements are extended to dynamic hopping experiments to show the accuracy of the dynamic models discussed in the Chapter 3.

Mechanism contains an actuation unit of GhostRobotics on the body. It is a T-Motor U10 80 kV, 1200 W brushless DC motor embedded with a motor driver unit. Motor driver has EtherCat communication interface and it can be controlled in torque and position control modes. Leg links are 3D printed with ABS plastic material with an FDM printer. Links have eye-fork type end structure and they are interconnected with bearings from two sides to construct revolute joint with low friction and minimized moment loads. Mechanism contacts ground via radial ball bearings that are fit on the leg to have a point contact convenient to the considered dynamic models. Body of the mechanism is constrained in the vertical direction by a linear bearing that connects body to a guide rail and the toe is constrained with a 3d printed guide located at the ground. Although the motor unit has high resolution absolute encoder that provides angular position and velocity, when the system goes into flight phase angular position of the motor does not provide information about the vertical position of the mechanism. For that purpose, a $2000cpr$ incremental encoder is integrated on the body of the mechanism. Angular information obtained from this encoder is converted to linear position and velocity by a 3D printed rack and pinion couple with a resolution of $0.09mm$. A contact switch is placed at the bottom to identify the stance-flight transi-

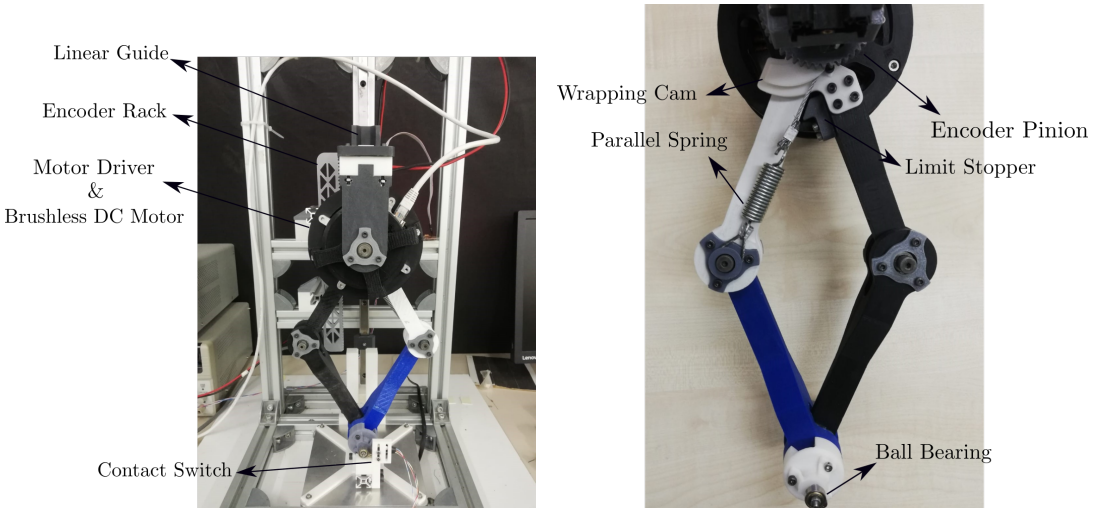

(a) Front view (b) Back view

Figure 4.1: Experimental hopper setup

tions. Overall communication structure is depicted in Figure 4.2. System is controlled with Simulink Real-time running on a x86 target computer. A Copley-Accelnet servo motor driver module is used as the data acquisition device. Despite the fact that this module is a motor driver, we only use the general purpose input-output pins to obtain auxiliary sensory input from the contact switch and the height encoder. Communication is done through EtherCat protocol at 1kHz sampling rate. Simulink target PC is the main controller and acts as an EtherCat master. Data acquisition device and the motor driver act as EtherCat slave to provide sensory feedback to the controller and receive torque/position command for the motor.

4.1 Vertical Hopping Control

System is controlled with a predefined cyclic open-loop torque input. As the parallel spring creates a dominant force along the motion trajectory, input torque should be in sync with the linear velocity of the system to obtain a smooth hopping motion. This can also be interpreted as exciting a system with its natural frequency. One should note that torque input is effective only in the stance phase to change the momentum of the system. Therefore, period of the input starts with the touch down instant of

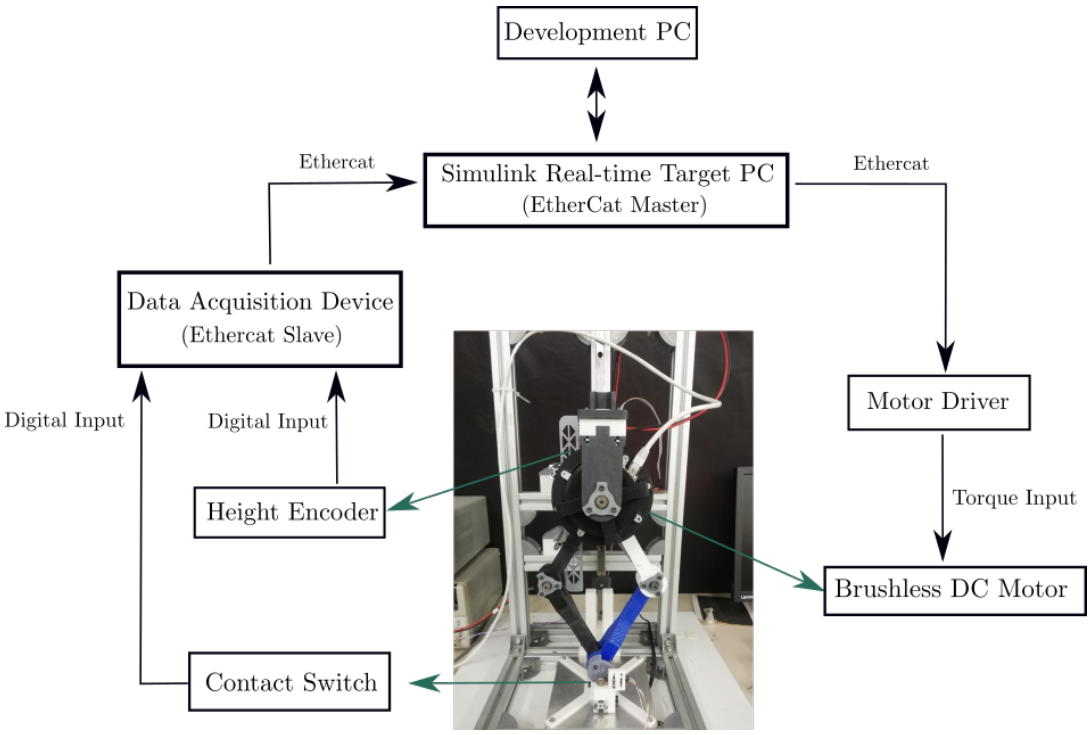

Figure 4.2: System connection

the system. Two main input profiles that can easily be applied in the experiments are defined as:

- Harmonic input,

$$\tau = \begin{cases} Tsin(\frac{t}{P}2\pi) & \text{, stance} \\ 0 & \text{, flight} \end{cases}$$

  Where T is the amplitude of the torque in N/m, P is the actuation period in seconds and t is time. Cycle of the actuation should be updated with the touch down instant

$$\tau = Tsin(\frac{t - t_d}{P}2\pi) \tag{4.1}$$

  Where t_d refers to the instant of touch down.

- Constant input

$$\tau = \begin{cases} Tsign(\dot{z}), \text{ stance} \\ 0 \quad \text{, flight} \end{cases}$$

  Where the $sign(\dot{z})$ implies the direction of the linear velocity of the body.

Figure 4.3 shows that both input profiles result in a dynamically stable hopping trajectory. As the input torque is updated according to the contact state of the system, it is important to identify the touch-down and lift-off instances. Signal of mechanical switch placed at the bottom is used to understand whether the toe is in touch the ground. Although, in theory, contact transition occurs instantly, in reality leg bounces back at the touch down instant with a high frequency and the switch reports multiple state transitions. To eliminate the false transitions, Algorithm 1 is used to obtain flight to stance transitions.

Algorithm 1 Algorithm to understand flight to stance transition

```
if phase = flight then
    if switch[t] = switch[t − 1] = 1 then
        phase ← stance
    end if
end if
```

Where $switch[t]$ indicates the state of the digital switch at time t. Rather than relying only on the switch reading, algorithm also checks the previous switch state to eliminate bouncing transitions.

Another restriction of the mechanical switch is the early or delayed transition detection within the $\pm 10ms$ range. Figure 4.4 is an example of the early touch down detection. As the touch down impact disrupts the monotonic decrease in the COM velocity during the flight phase, one can clearly determine the real touch down instant occurring about $5ms$ later than the detection of the switch. This early/delayed phase transitions are due to the imperfect location of the switch and could not be improved without changing the sensor. Contact detection is a common challenge in legged robotics, deserving more detailed effort specific to the platform. In the context of this study, overall performance will be evaluated disregarding the error introduced in the switch. As mentioned in the setup description, both the encoder of the motor and the auxiliary height encoder can be used to obtain COM height and leg angle. However, unpredicted errors in the phase transition instants due to the switch make it difficult to use the motor encoder. Therefore, height encoder is used as the only source of information for leg angle/velocity and the COM position/velocity.

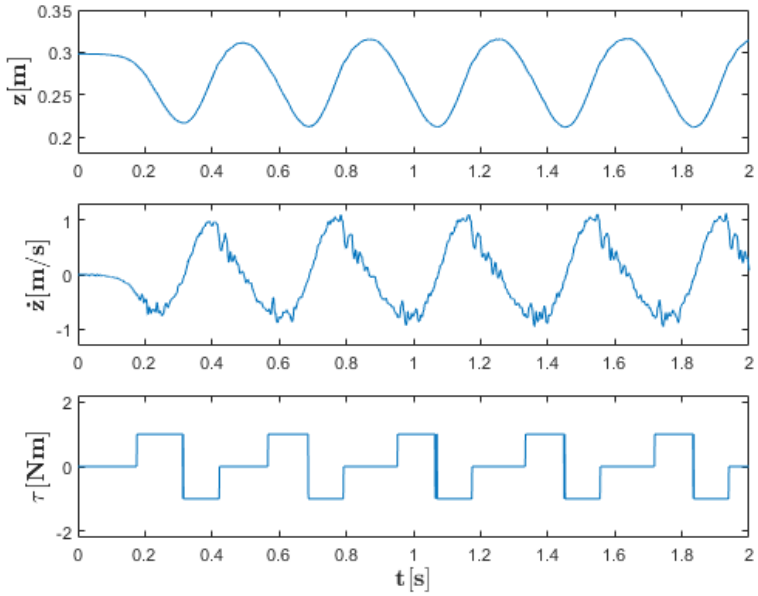

(a) Step-wise constant input

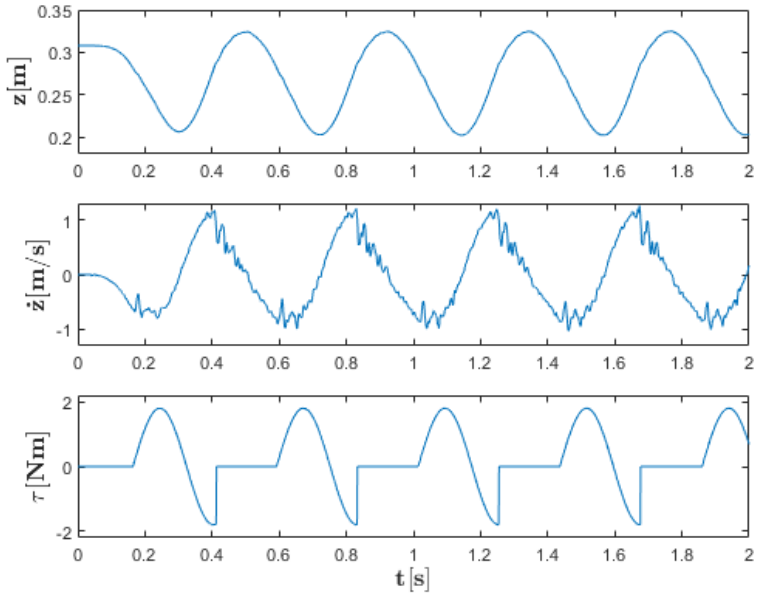

(b) Harmonic input

Figure 4.3: Continuous jump trajectories with two different open loop torque input profile

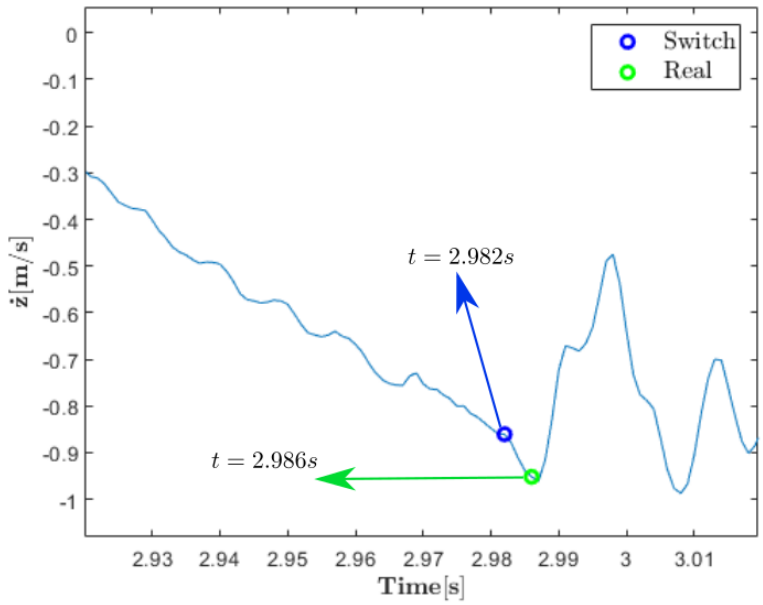

Figure 4.4: COM Velocity w.r.t time with a focus on the touch down instant

4.2 Parameter Estimation and Cross Validation

This section is concerned about the identification of the physical system parameters. While it is possible to use the physical parameters obtained from the CAD model and separate measurements of each component like link lengths, masses etc., this approach tends to produce inaccuracies for some reasons. Firstly, it is difficult to model all minor components like bolts, nuts and inner components of the off-the-shelf components like electrical motor and guiding rails. Since the equation of motion of the system depends not only on the inertial parameters but also on center of mass of the assembled components, lack of these components in the model increases the inaccuracy. In addition to that, it is very difficult to have an accurate guess about the friction losses. As the main concern is the overall performance of the model based controllers in the hardware platform, adopted method for identification is fitting physical parameters to dynamical model by using the experimental data. The main idea is to find a set of physical parameters that minimizes the difference between the simulated and measured output states. Similar to the dynamic formulation of the system in discrete domain described in 3.8, states can be formulated as a function of

the parameters.

$$x[n+1] = f_\alpha(x[n], u[n]) \tag{4.2}$$

Where, α is a vector of parameters. For simplicity, rather than defining a new output state vector $y[n] = g_\alpha(x[n], u[n])$, take state vector $x[t]$ as the output states. So, using a least squares formulation, the optimization objective becomes:

$$\min_{\alpha} \sum_{n=2}^{N} ||x[n] - x_m[n]||^2 \tag{4.3}$$

Where, x and x_m refer to the estimated and measured states, respectively. N is the number of total measured states. Note that, operator $||\ ||$ implies 2 norm. 4.3 can be held with two distinct approaches. The first is to minimize one step prediction error and the second is to minimize the overall simulation error. Both methods use 4.3 as the cost function. However, estimated state differs as follows:

$$x[n+1] = \begin{cases} f_\alpha(x_m[n], u[n]), \text{ equation error method} \\ f_\alpha(x[n], u[n]), \text{ simulation error method} \end{cases}$$

Difference between the two methods is that in equation error method each state is estimated using the previously measured state disregarding the previously estimated state. Whereas in the simulation error method only the initial state is taken from the experiment and then all of the states are estimated sequentially.

In practice, simulation of the dynamic model that is of concern is used to obtain the states in the optimization objective described in 4.3. COM position and velocity, z and $\dot{z}$ are the two states to be estimated and whose direct measurements are available. Only one step hopping trajectories are considered. Parameters regarding the stance and flight phases are estimated separately using distinct initial conditions from the given experimental trajectory. Then, fixing the physical parameters for each phase, impact parameters can be found to complete the set of parameters that generates the most accurate overall hopping motion. $fmincon$ method of the MATLAB carries out repetitive simulations until it finds a set of input parameters that minimize a given cost function regarding the experimented and simulated states. For the hopping motion, cost function is set as the sum of the normalized mean square errors in COM position and velocity trajectories.

$$J = \frac{||z_{exp} - z_{sim}||^2}{||z_{exp} - \bar{z}_{exp}||^2} + \frac{||\dot{z}_{exp} - \dot{z}_{sim}||^2}{||\dot{z}_{exp} - \bar{\dot{z}}_{exp}||^2} \tag{4.4}$$

Where, subscripts exp and sim refers to the experimented and simulated trajectories respectively. And, $\bar{z}$ and $\bar{\dot{z}}_{exp}$ are the mean values of the experimented COM position and velocity. This cost function aims to minimize the tracking error both in the position and the velocity. Figure 4.5 illustrates an example single stride experiment used for parameter estimation and validation. Initial condition of the estimation trajectory is selected near the transition point of the related phase. The noisy transition in velocity just after the impact instants encircled in the Figure 4.5b. Preliminary results indicated that the initial condition significantly affects the validation results. Even if a sensible set of parameters are found, simulated trajectories deflect from experimental with the noisy initial condition. Therefore, the velocity profile is filtered at a $15Hz$ cut-off frequency with a third order butterworth filter using the $filtfilt$ method of MATLAB. This method eliminates the phase shift resulting from the filtering by processing the data both in forward and backward directions. Cut-off frequency of the filter is chosen by iterations with a focus on not distorting the main character of the trajectory especially in the phase transitions where a more abrupt change occurs. An example filtered velocity profile can be seen in Figure 4.6. One can notice that after the transitional effect of the impact ends stance phase velocity does not require significant filtering. Therefore, only for the estimation of stance phase, raw velocity data is used. Initial point is selected as a point where the impact vibration is died.

For each phase, multiple single stride hopping experiments are done and the overall objective function is set to find the parameters that results in the best fit for the all of the experiments. So, the overall objective becomes:

$$\min_{\alpha} \sum_{i=1}^{i=N} J_i \tag{4.5}$$

Only the harmonic input profile described in 4.1 is considered. Constant input profile causes abrupt torque changes that may result in inaccuracies, and thus discarded. For statistical consistency, k-fold cross validation method is used to estimate and validate the parameters. This method ensures that a data set is not used in validation if it is used in estimation for unbiased validation results. Also, each experiment trajectory is used $(k-1)$ many time for estimation and only once for validation. Same experiment set is considered both for the linear and non-linear models.

Although it is not feasible to directly obtain all physical parameters from measure-

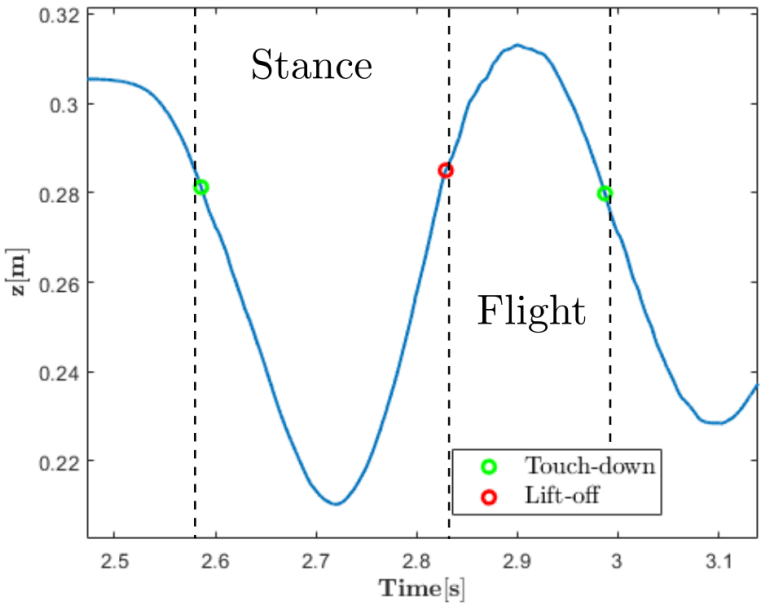

(a) COM position trajectory

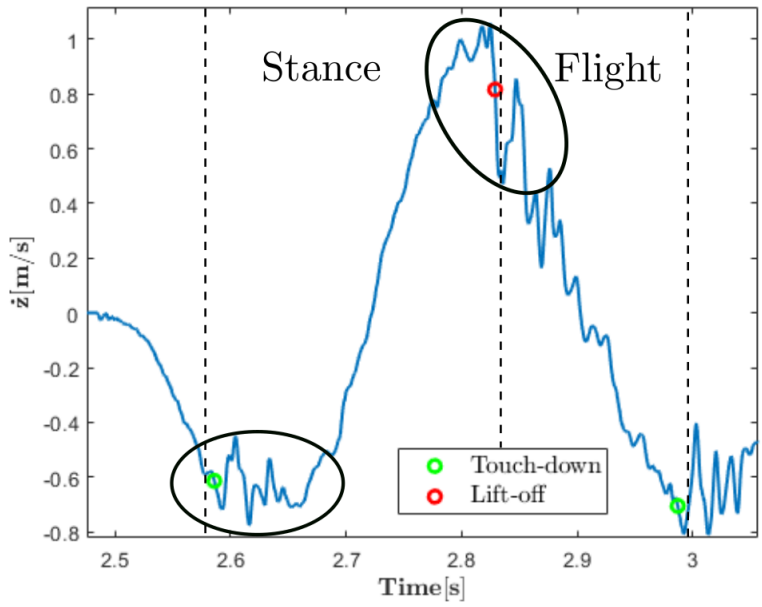

(b) COM velocity trajectory with a focus on impact transitions

Figure 4.5: Single stride hopping data for parameter estimation. Dashed lines separate different phases.

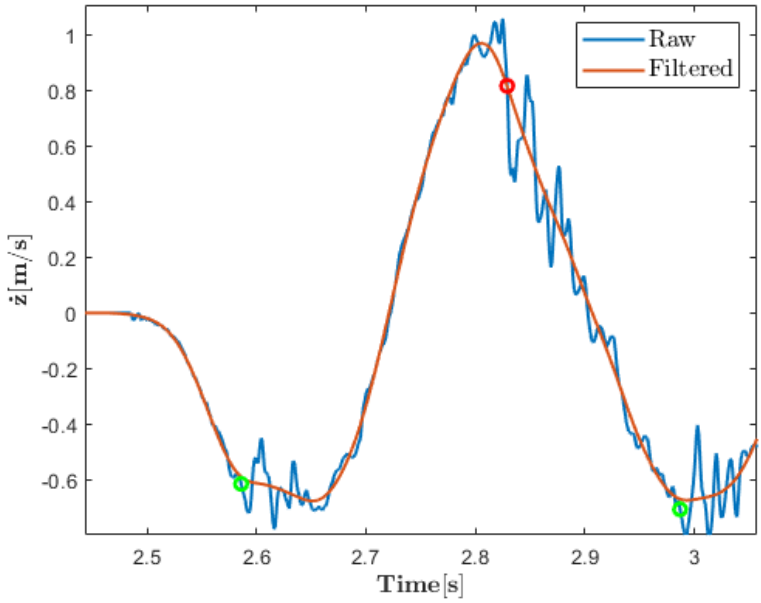

Figure 4.6: Filtered COM velocity

ments, using measured parameters wherever possible is beneficial to decrease the number of variables to be estimated. Also, constraints can be set in optimization process to obtain physically consistent parameters. Total mass of the system and the spring constant are the two lumped quantities that can be measured with relatively high accuracy. Total mass of the leg is measured to be $1.62kg$. And the equivalent spring constant is measured by using a force plate following the procedure in [1]. Ground reaction force is measured at discrete deflection points with a AMTI he6x6 force plate and a linear line is fit to the points as shown in 4.7. Equation of the best fit line is $605N/m + 2.7N$. The offset force is associated with the pretension force of the tension spring in [1].

However, with a careful examination, it is observed that the parallel spring transmits only the weight of the upper portion of the mechanism where the weight of the lower links also contributes to the measured ground reaction force as depicted in Figure 4.8. Total mass of the lower portion of the mechanism, including the all assembly elements and bearings is measured to be approximately $0.2kg$. Therefore, a large portion of the offset force is coming from the dead-weight of the lower links. Pretension force of the tension spring estimated to be lower than $1N$ is neglected in the dynamical models

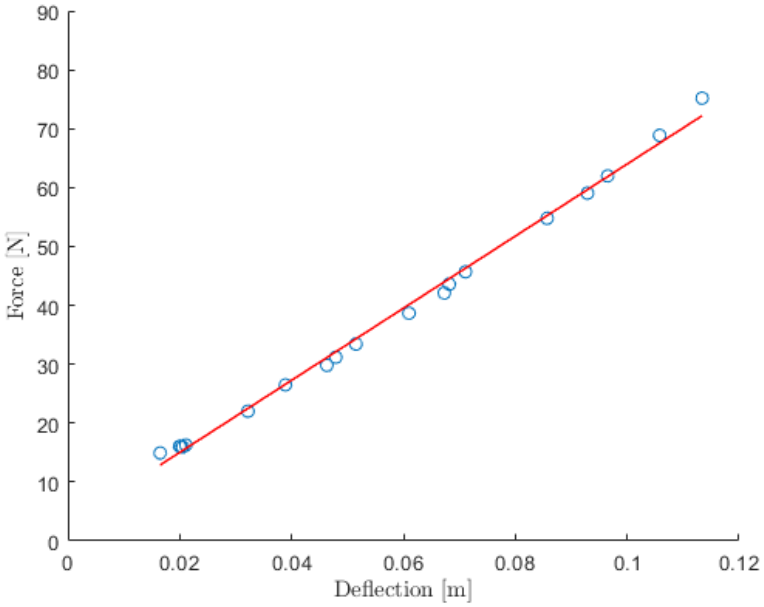

Figure 4.7: Measured vertical spring force

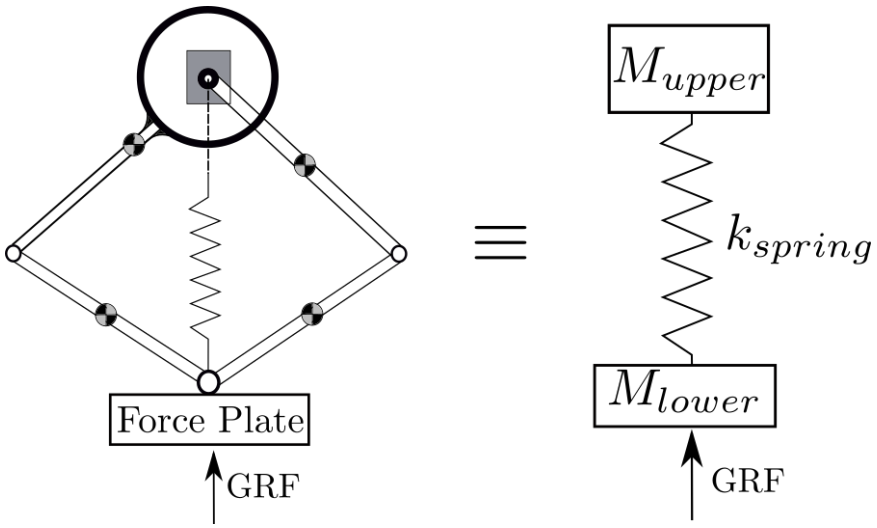

Figure 4.8: Schematic for the spring force measurement model

during the parameter estimation process.

4.2.1 Estimation and Validation Results

4.2.1.1 Linear Model

Dynamics of the stance phase is described in equation 3.5. Known parameters are selected as:

$$k = 605N/m$$
$$g = 9.81m/s^2$$
$$z_0 = 0.289m$$

Parameters to be estimated are the damping coefficient d and the lumped body mass m. 60 experiments with different excitation period and amplitude is considered for the stance phase. 10 fold cross validation scheme is used for estimation and validation. Distribution of the estimated parameters are reported in Figure 4.9. Main character of the linear mass-spring-damper system is described by its natural frequency. In that case, damped natural frequency can be found as:

$$\omega_n = \sqrt{\frac{k}{m}}$$
$$\xi = \frac{d}{2\sqrt{km}}$$
$$\omega_d = w_n\sqrt{1-\xi^2}$$

Damped natural frequency distribution derived from the estimated mass and damping values with both simulation and estimation error methods are presented in Figure 4.10. One can see the validation results in Figure 4.11. In addition to the normalized mean square errors in COM position and velocity, that are actually the minimized cost function of the optimization, mean absolute error which gives a more direct idea about the tracking performance is also reported. In Figure 4.12, two example trajectories for different validation results are presented to provide a better interpretation of the validation errors.

Dynamics of the flight phase is described in equation 3.6. In the free fall, as the all of the system accelerates as a whole, lumped mass assumption is relatively more accurate. Therefore, mass of the system is taken from the weight measurement. Known

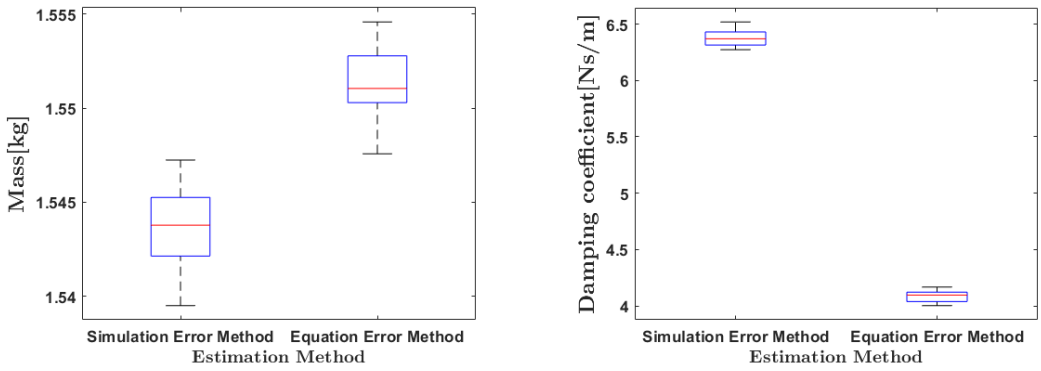

(a) Estimated lumped mass

(b) Estimated damping coefficient

Figure 4.9: Distribution of estimated parameters for stance phase

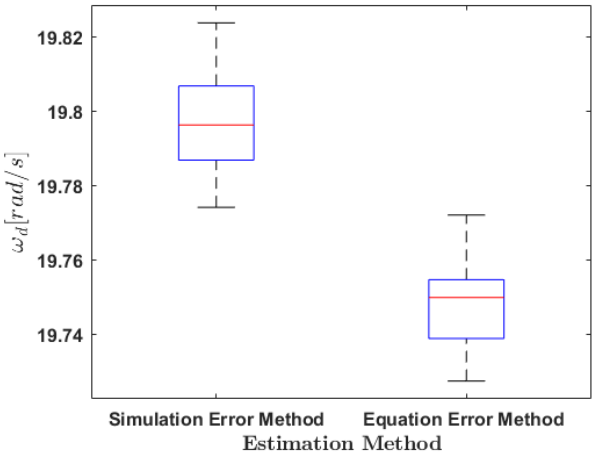

Figure 4.10: Distribution of estimated damped natural frequency

parameters are selected as:

$$g = 9.81 m/s^2$$

$$m = 1.62 kg$$

Only parameter to be estimated is the damping coefficient of the flight phase, d_f. As there is no actuation input in the flight phase, initial conditions determines the motion trajectory. Effective inputs are more restricted compared to the stance phase, and increasing number of experiments observed to affect cumulative results less. 20 experimental trajectories are taken and 5 fold cross validation is used for estimation and validation. Distribution of the damping coefficient estimated with both simulation

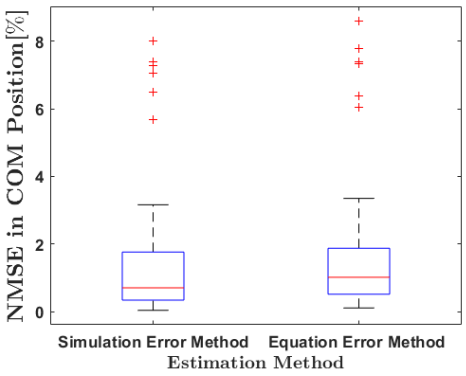

(a) Normalized mean square error in COM position

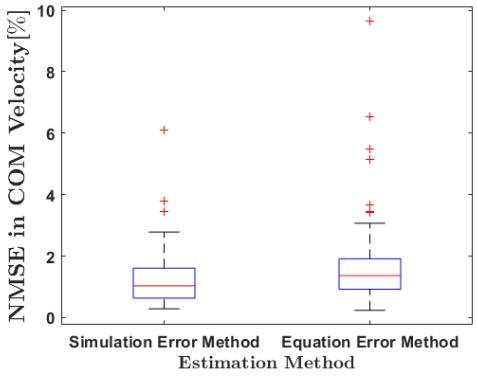

(b) Normalized mean square error in COM velocity

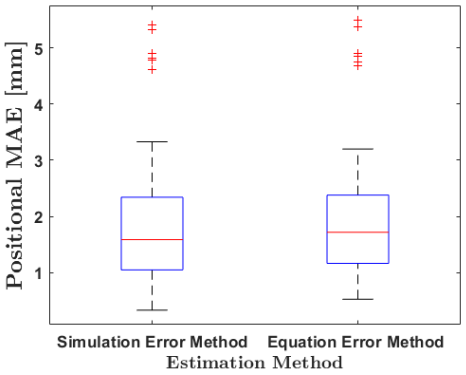

(c) Mean absolute error in COM position

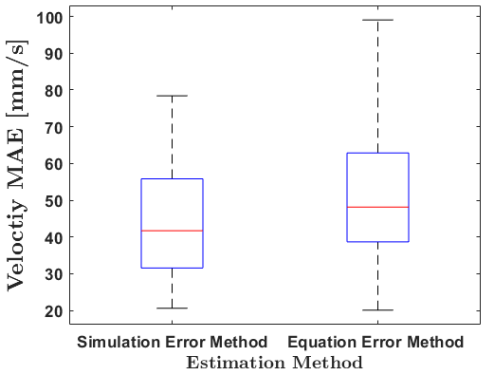

(d) Mean absolute error in COM velocity

Figure 4.11: 10-Fold Cross validation of the estimated parameters for stance phase of the linear model

and one step prediction error methods is reported in Figure 4.13. As in the stance phase, validation error distributions are presented with boxplots in Figure 4.14. Two of the example trajectories with different validation errors are presented in Figure 4.15.

By having parameters that predict the isolated stance and flight phases accurately, what is left to have an accurate model of the complete motion is having the impact parameters of phase transitions. Overall equation of motion in discrete domain is described in 3.8, and the impact model is given in 3.9. To estimate the impact parameters, mean values of the estimated stance and flight parameters are fixed. Since

overall simulation of the motion including the transition of the dynamics is considered, it is not possible to isolate a portion of the trajectory and directly apply the experimental inputs in the simulation. When estimating stance and flight phases, both the simulation and the experiment trajectory are known not to change their phase for sure. So, with a given initial condition we are confident to use the experimental input in the simulation. However, in the overall model simulation and experiment does not experience phase change at exactly the same instant. Also, time shift in the transition instants caused by the contact switch increases the inaccuracy. Therefore, only the simulation error method is used discarding the one step estimation error method and the torque input is predefined in the simulation to be started with the predicted contact instant. By considering the validation results for stance and flight phase, known parameters are selected as:

$$k = 605N/m$$
$$m = 1.554kg$$
$$d_s = 6.42Ns/m$$
$$d_f = 1.18Ns/m$$
$$g = 9.81m/s^2$$
$$z_0 = 0.289m$$

And, the parameters to be estimated are the α_{lo} and α_{td} which describe the discontinuous velocity change during the lift-off and touch-down phase transitions. Distribution of the estimated parameters is presented in Figure 4.16. Distribution of the validation results is reported in the Figure 4.17. Figure 4.18 visualizes the different validation errors.

4.2.1.2 Non-Linear Model

In a compact form non-linear model described as in 3.11. Using constraint consistent dynamic formulation, physical parameters that shapes the equation of motion is given in 3.12. Non-linear terms result in tedious and long expressions, therefore, physical parameters of concern are lumped together. They are listed as:

- a: Combination of the inertial parameters related to all links

- b: Inertial parameters related to lower links
- e: Mass parameters of all links defining the total potential energy of all of the links
- m_{total}: Total mass of the system
- d: Damping coefficient related to the linear velocity of COM
- k: Equivalent virtual spring coefficient

One should not that, having a lumped dynamical model and the introduced data driven estimation method, it is not possible to identify the properties of each separate link. For example, one can not find the inertia of the upper link 2 alone. However, it does not harm the model's or the controller's validity as the isolated inertial properties of links do not affect the motion. Their combined effect is the main concern. MATLAB's $ode45$ method does not allow to adjust solution steps, thus, simulating the system directly with the experimental inputs is not possible. Therefore, only the simulation error method is used throughout estimation and validation. A predefined torque profile w.r.t time is used to excite the system in the simulation. As the flight phase dynamics is the same with the linear model, damping coefficient for flight phase, d_f is directly taken from the linear model. And, as the impact parameters are inherently dependent on the inertial parameters of the links, estimation is carried out only for the stance phase. The same 60 experimental trajectories used for the stance phase of the linear model is considered. Distribution of the estimated parameters with those 60 experiments and 10 fold cross validation can be seen in Figure 4.19 and the validation results are given in the Figure 4.20.

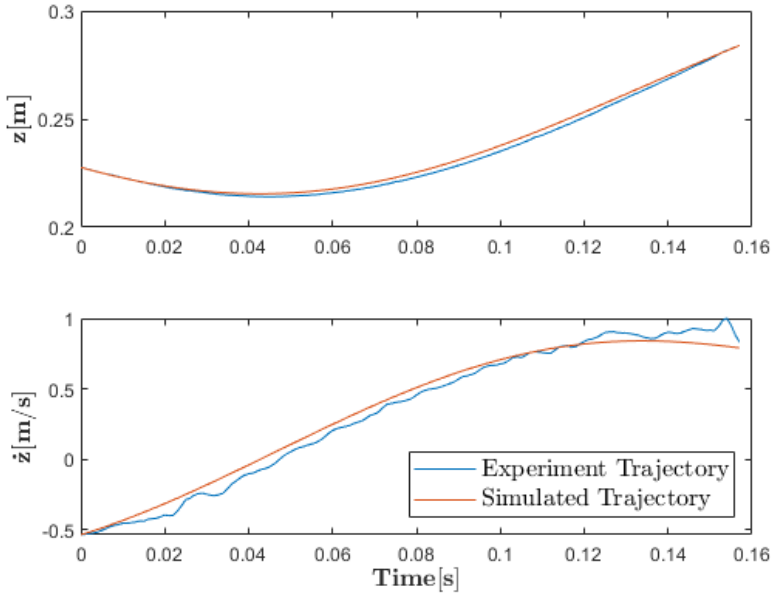

(a) Example trajectory 1

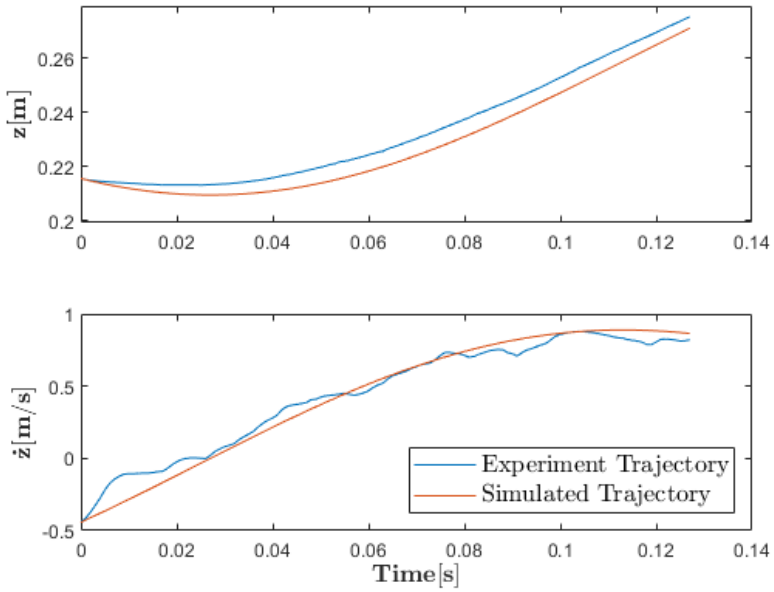

(b) Example trajectory 2

Figure 4.12: Sample trajectories with different validation error for the stance phase of the linear model. (a) NMSE in COM Position: 0.6%, MAE in COM position: $1.5mm$, NMSE in COM Velocity: 1.9%, MAE in COM velocity: $53.6mm/s$. (b) NMSE in COM Position: 6.8%, MAE in COM position: $4.8mm$, NMSE in COM Velocity: 2.6%, MAE in COM velocity: $54.6mm/s$

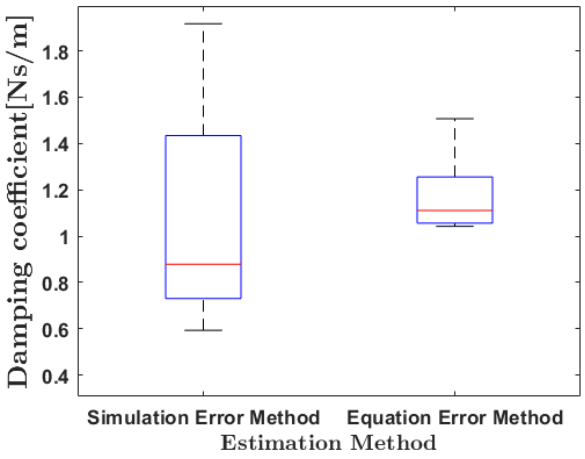

Figure 4.13: Estimated damping coefficient for flight phase

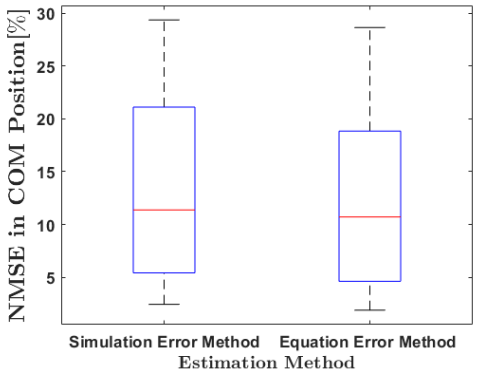

(a) Normalized mean square error in COM position

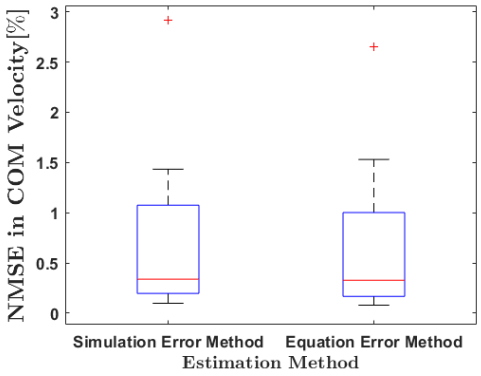

(b) Normalized mean square error in COM velocity

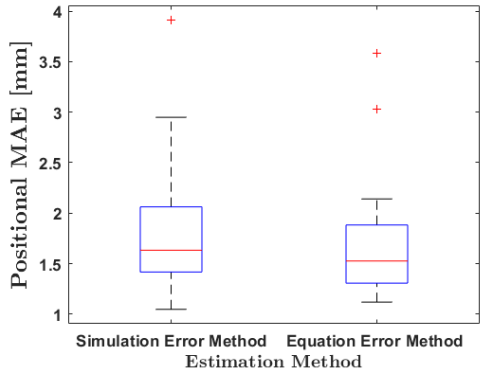

(c) Mean absolute error in COM position

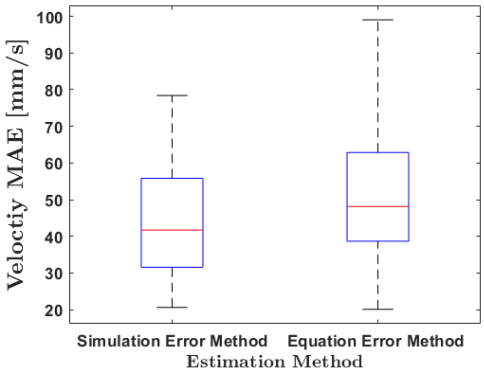

(d) Mean absolute error in COM velocity

Figure 4.14: 5-Fold Cross validation of the estimated parameters for flight phase

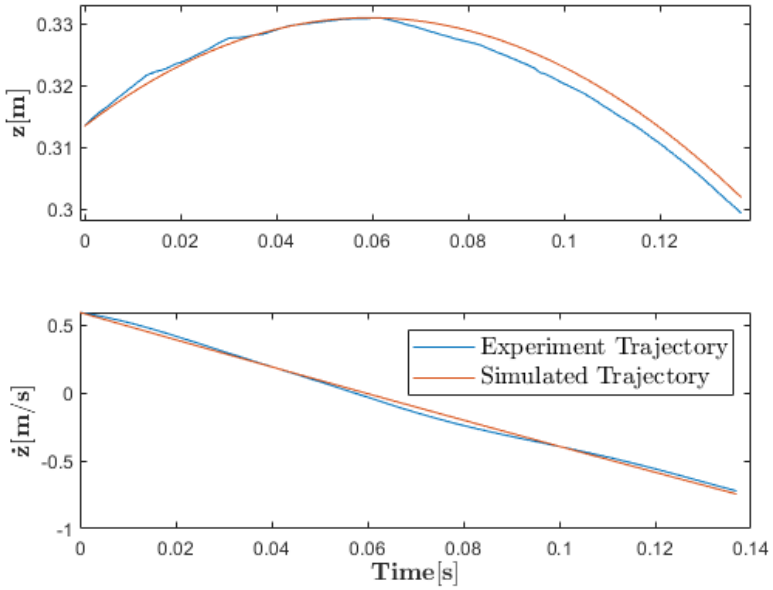

(a) Example trajectory 1

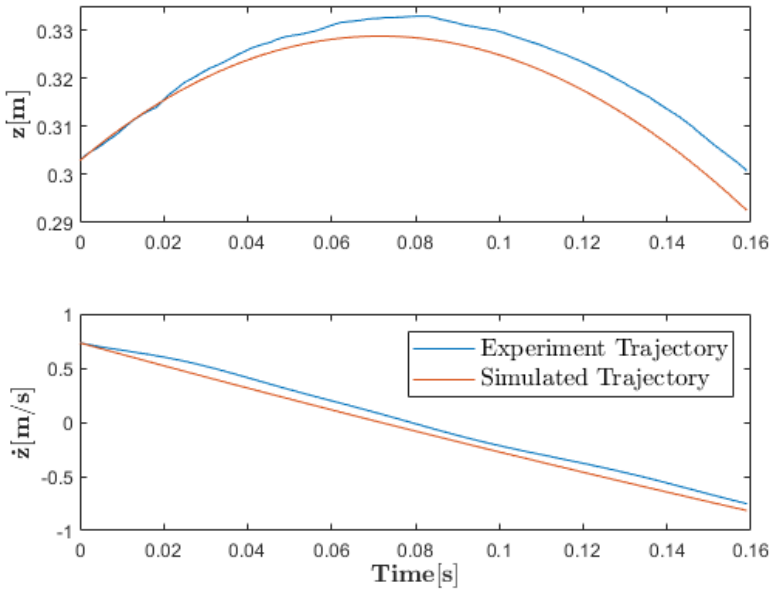

(b) Example trajectory 2

Figure 4.15: Sample trajectories with different validation error for the flight phase of the linear model. (a) NMSE in COM Position: 4.9%, MAE in COM position: $1.4mm$, NMSE in COM Velocity: 1.9%, MAE in COM velocity: $53.6mm/s$. (b) NMSE in COM Position: 6.8%, MAE in COM position: $4.8mm$, NMSE in COM Velocity: 3.7%, MAE in COM velocity: $20.8mm/s$

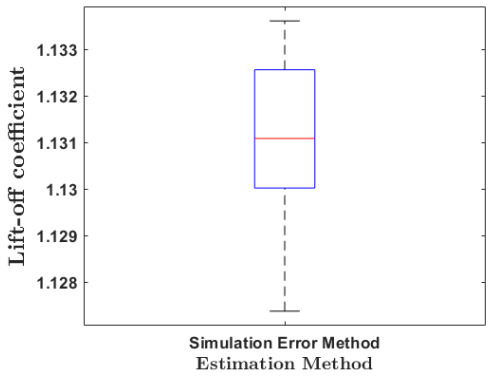

(a) Lift-off coefficient

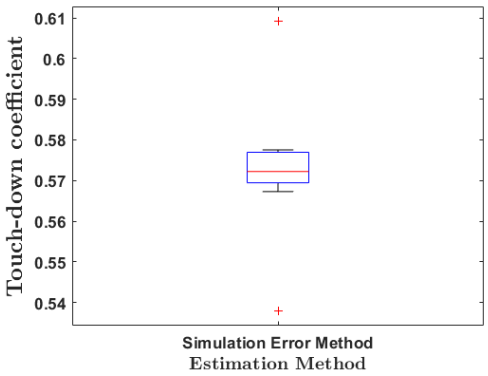

(b) Touch-down coefficient

Figure 4.16: Distribution of the estimated impact parameters

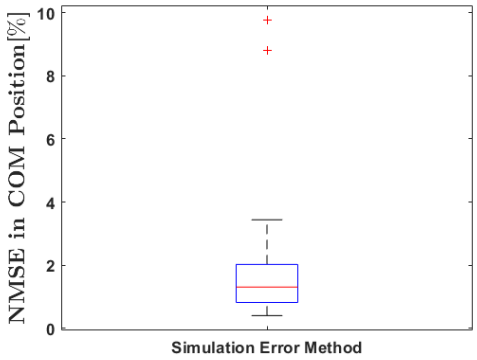

(a) Normalized mean square error in COM position

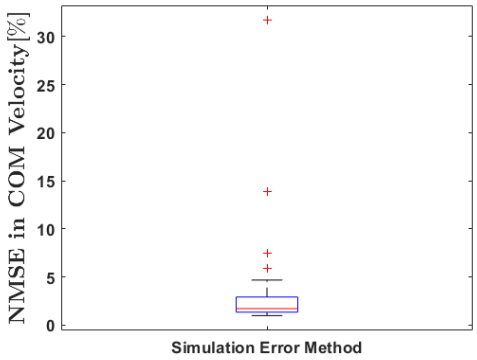

(b) Normalized mean square error in COM velocity

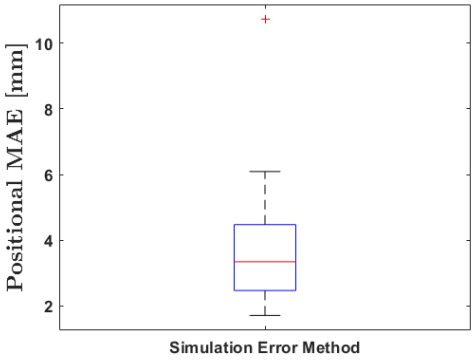

(c) Mean absolute error in COM position

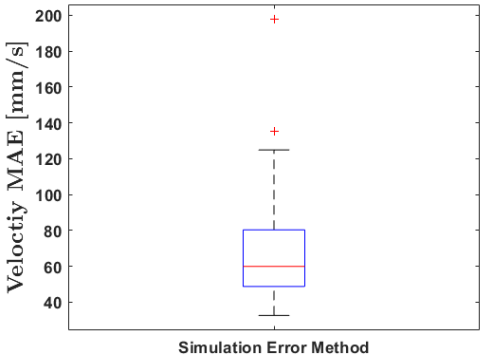

(d) Mean absolute error in COM velocity

Figure 4.17: 10-Fold Cross validation of the phase transition parameters

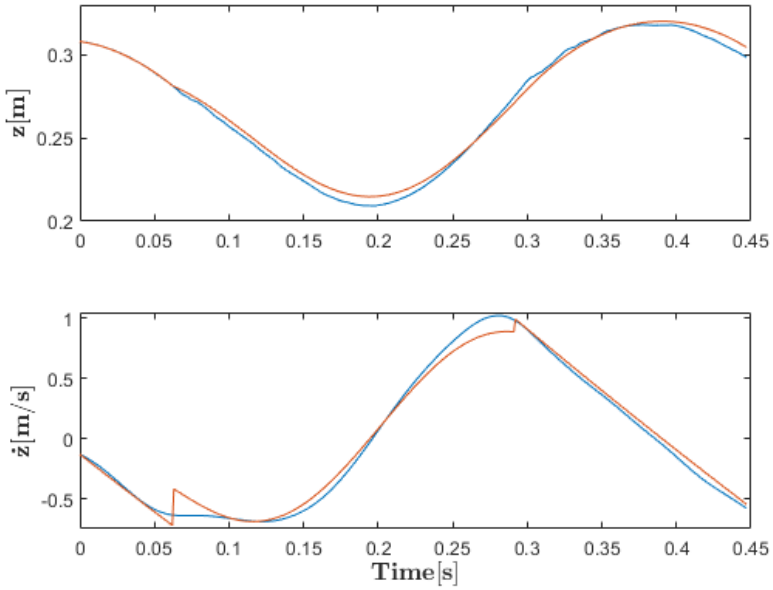

(a) Example trajectory 1

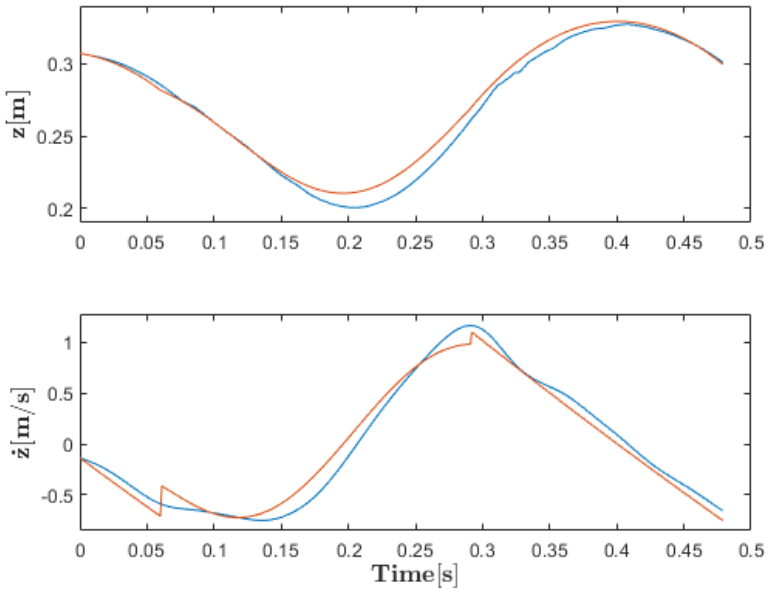

(b) Example trajectory 2

Figure 4.18: Sample trajectories with different validation error for the overall motion trajectory of the linear model. Blue: experiment, red: simulation. (a) NMSE in COM Position: 0.75%, MAE in COM position: $2.7mm$, NMSE in COM Velocity: 1.23%, MAE in COM velocity: $49.6mm/s$. (b) NMSE in COM Position: 2.1%, MAE in COM position: $4.7mm$, NMSE in COM Velocity: 2.9%, MAE in COM velocity: $89.1mm/s$

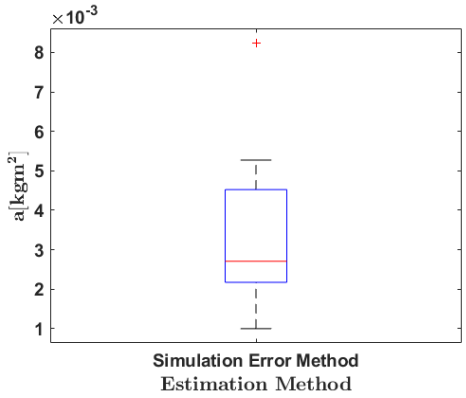

(a) Normalized mean square error in COM position

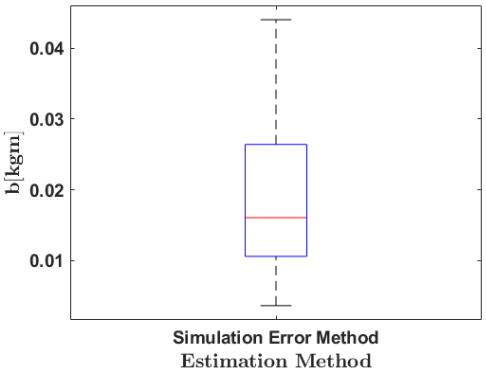

(b) Normalized mean square error in COM velocity

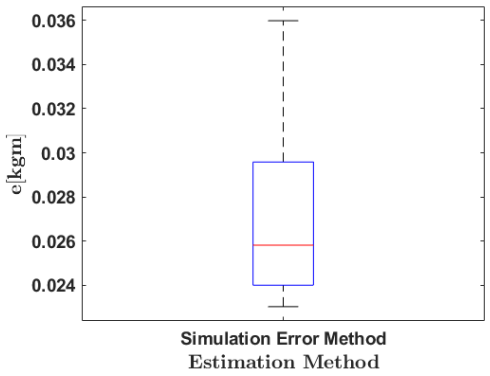

(c) Mean absolute error in COM position

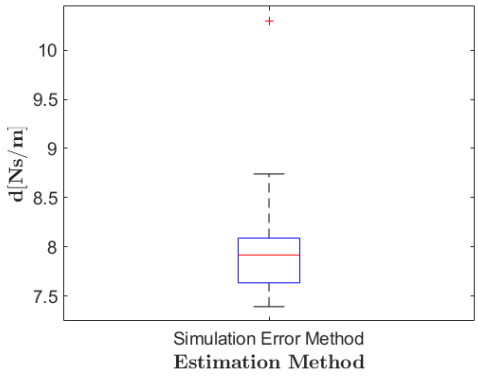

(d) Mean absolute error in COM velocity

Figure 4.19: Distribution of the estimated parameters for the stance phase of the non-linear model

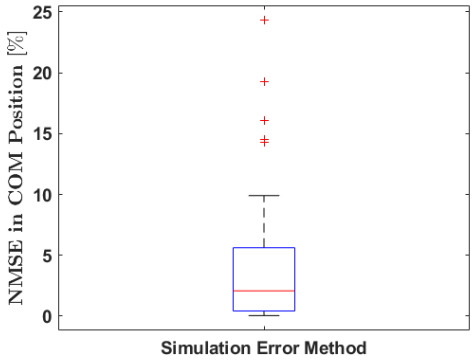

(a) Normalized mean square error in COM position

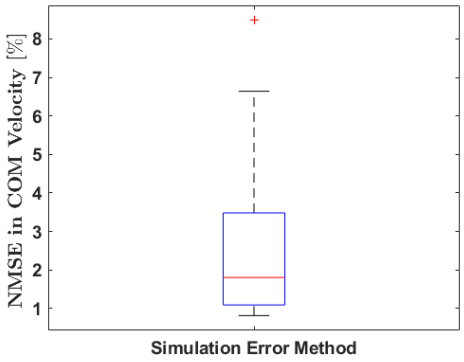

(b) Normalized mean square error in COM velocity

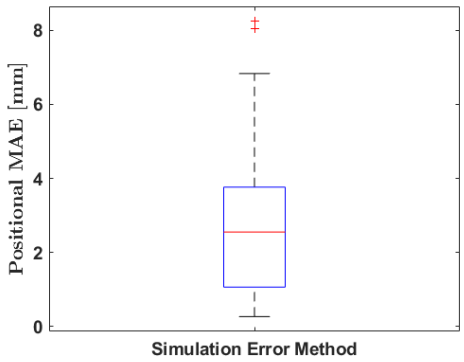

(c) Mean absolute error in COM position

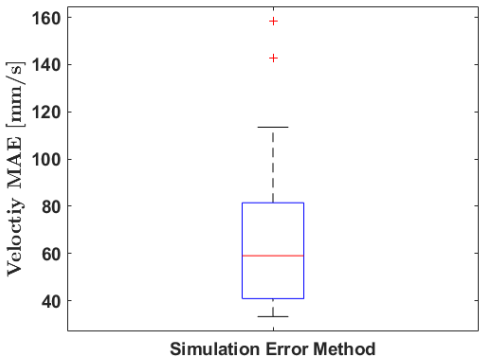

(d) Mean absolute error in COM velocity

Figure 4.20: 10-Fold Cross validation of the estimated parameters for stance phase of non-linear model

CHAPTER 5

CLUTCH DESIGN

Modeling and experimental verification studies in Chapter 3 and Chapter 4 show the relevance of the designed parallel elastic hopping mechanism for the intended controllers. However, despite the performance of the dynamic running and hopping behavior of the mechanism, practical application of the parallel elastic actuation in a robot platform involves joint mobility problem. This chapter details the design of a clutch mechanism to solve the joint mobility problem and to increase the overall energetic efficiency.

5.1 Working Principle and Conceptual Design

Addressing the problems related to clutch mechanisms reported in the literature and considering the aimed controller models, design requirements of the clutch mechanism are listed as :

- Clutch should be able to hold large forces during the locomotion cycle

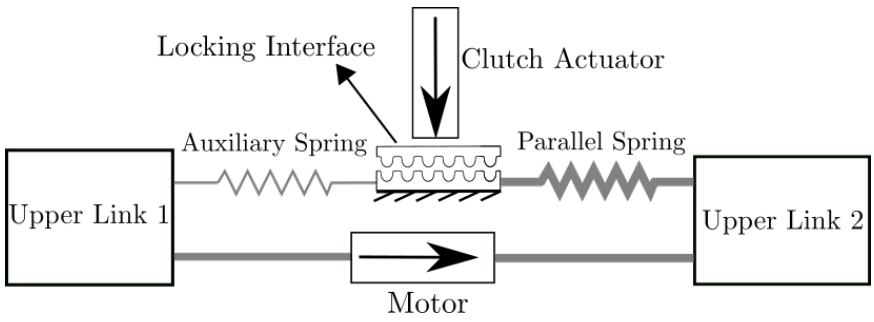

Figure 5.1: Working principle of the clutch

- Engage/disengage action should be fast enough in order not to interfere the locomotion
- Distortion of the joint motion during the disengagement due to the possible sticking should be eliminated
- With the integration of the clutch, legged system should preserve its passive dynamic structure for the desired controllers

Working principle of the switch mechanism utilized in the SPEAR robot [30] is adopted for the design of the clutch. This mechanism provides a practical solution for elimination of the parallel spring and re-activation of it at a predefined position by the usage of an auxiliary spring. Working principle is illustrated in Figure 5.1. In the free configuration equivalent spring coefficient is negligible due to the soft auxiliary spring, however, when the actuator fixes the point in between only the parallel spring operates. Following the criterion for the design requirements, an embodiment of the described working principle is presented in the Figure 5.2 as a concept. A solenoid actuator integrated with return springs provides rapid linear motion since a force/-torque transmission is not involved. As the parallel spring is active when the solenoid is off, clutch does not consume energy to benefit from the spring. To avoid a discrete engagement interface, timing belt is selected as the locking interface placed opposed to a key profile. As most of the timing belt profiles contain very small and elastic teeth, engagement action is expected to be close to the continuous. Disengagement action depends on the tooth height of the timing belt: when the actuator pulls back the pressing shaft in the order of the tooth length, two matching profiles are expected to be separated as depicted in Figure 5.2a. Using a timing belt as the locking interface increases the effectiveness of using a solenoid actuator. Force capacity and the response time of the solenoid improve with the square of the stroke length. Therefore, having a small tooth profile in the locking interface makes room to optimize the solution with a solenoid actuator. In contrast to the SPEAR robot, proposed concept locates the clutch on the body. This serves to preserve the small mass and inertia of the legs and helps to reduce impact losses. Also, having light-weight legs with concentrated mass on the body is more suitable for realizing SLIP like controller models.

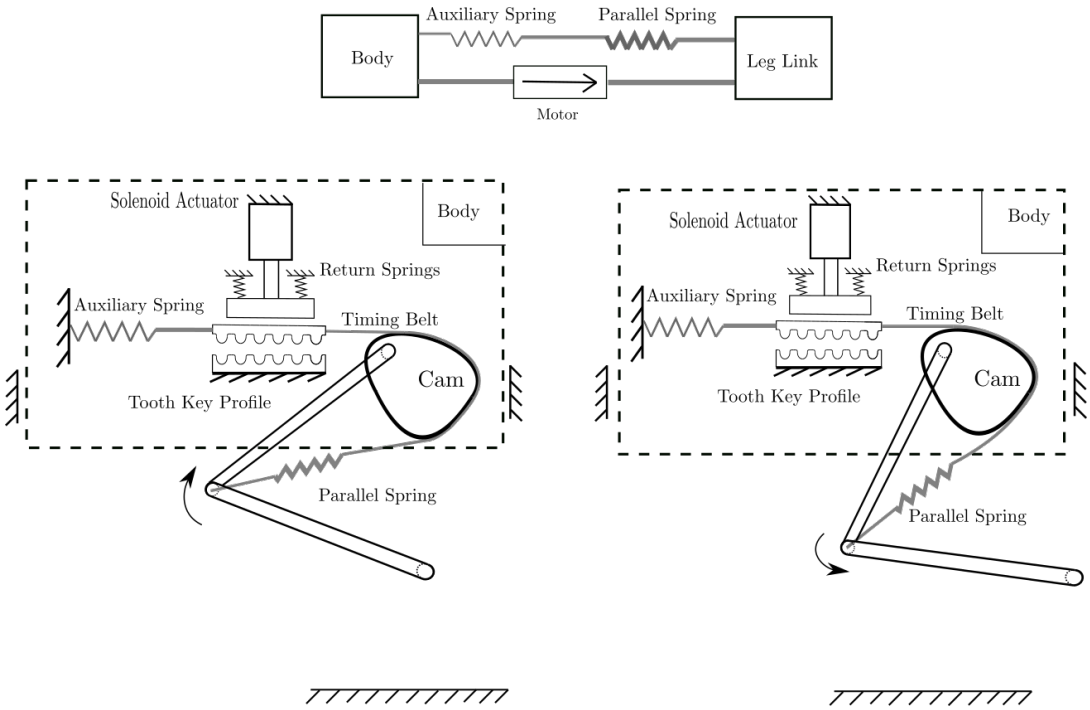

(a) Flight phase

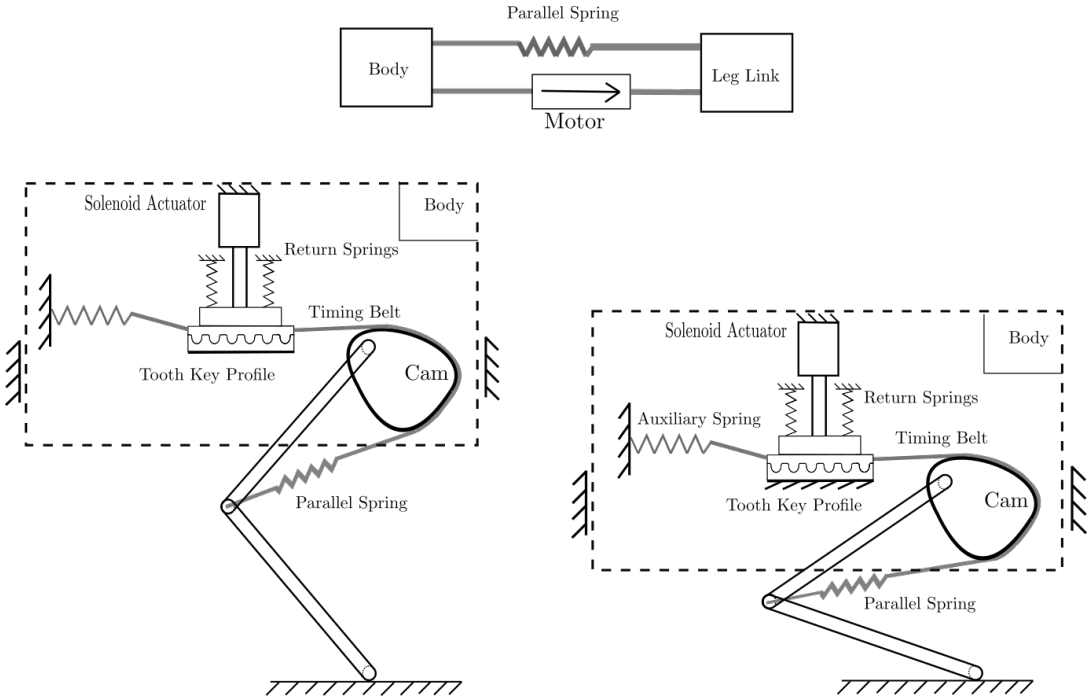

(b) Stance phase

Figure 5.2: Concept design of the clutch mechanism

In order to test the holding capacity and the engagement/disengagement performance of the proposed concept, a preliminary test setup shown in Figure 5.3a is designed. M3 belt profile is preferred due to its ease of availability. It has approximately $1.8mm$ tooth height that will be important for deciding the stroke length/force capacity of the solenoid. Pressing shaft of the solenoid and the key profile are designed to be 3D printed. Teeth profile of the key is simply the negative of the timing belt. Ladex B14-L-258-B-4 model latching solenoid that can apply almost $20N$ force from $2.5mm$ stroke is utilized in the setup. The solenoid is reported to have $0-20ms$ response time under no load condition. During the preliminary tests, it is observed that the holding capacity of the clutch significantly increases as the pressing shaft exerts larger forces. Also, increasing number of engaging tooth of the key improves the holding load. However, as the return springs become stiffer to provide larger forces, solenoid needs to have a larger force capacity, and thus it gets larger and heavier. Having a larger matching surface on the key section, also, requires larger area in the mechanism. In conclusion, there is a trade-off between the achievable holding torques and the compactness/weight of the mechanism. In order to determine the force requirement of the return springs in a systematic manner, solenoid of the test setup is replaced with a mechanical interface on which dead weight can be inserted. As shown in Figure 5.3b. Different dead-weights on the mechanism represents the pushing force of the return springs. Tests with different dead-weights shows almost linear relation between the pushing force and the amount of load that can be hold through the timing belt without slipping.

Trade-off between holding force and compactness results in an iterative design process to select a suitable return spring and a solenoid. Optimizing a coil spring for that purpose requires significant effort, since the spring constant and available force/stroke length differ with many parameters like spring diameter, coil diameter, overall length and the material properties. Moreover, finding off-the shelf coil spring at each desired dimension is not possible. For that reason, orthoplanar spring (OPS) concept [31] is utilized in the design instead of a traditional coil spring. One can see an OPS that is 3D printed with ABS material from an FDM printer and integrated in the setup in Figure 5.4. Center part of the OPS is connected to the outer wall with 3 cantilever beams. Bending profile of the beams determines the equivalent stiffness of the center of the

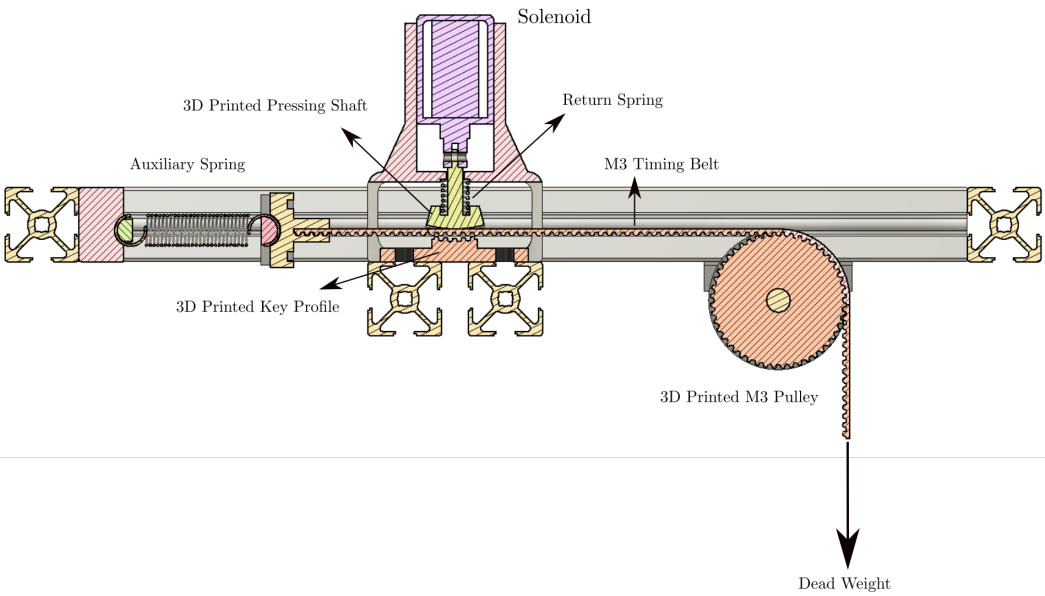

(a) CAD model of the preliminary test setup

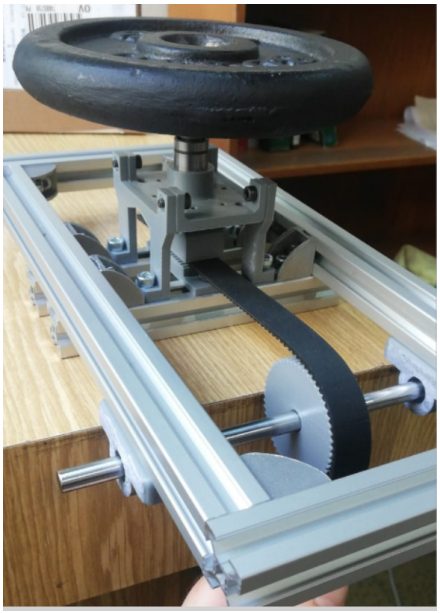

(b) Static load testing setup

Figure 5.3: Preliminary test setup for the clutch mechanism

(a) 3D Printed orthoplanar spring

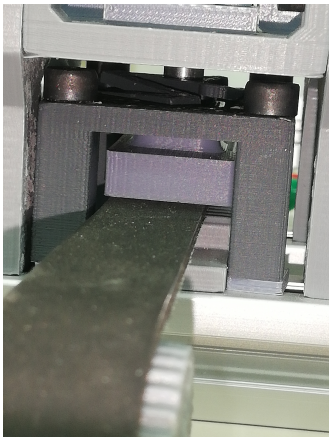

(b) Orthoplanar spring integrated to the test setup

Figure 5.4: Usage of the orthoplanar spring

OPS in the outward axial direction. Since the bending stiffness of the cantilever beam structure increases dramatically with the increasing beam thickness, a wide range of stiffness values can easily be achieved with small amount of change in the thickness $(0.5 - 3mm)$.

In addition to the OPS, a rotary encoder with $2400count/rev$ is integrated to the shaft carrying the M3 pulley shown in Figure 5.3a. Arduino UNO micro-controller board is used to control the solenoid through a MOSFET motor driver card. It also samples the encoder signal at a fixed rate of 250 Hz. This setup is shown in the Figure 5.5. To conduct a release/catch experiment, firstly a static load is hanged on the free and of the timing belt. While the system stays stationary with the passive force of the OPS, with the keyboard input of the user, Arduino sends release signal to the solenoid driver. As the solenoid releases the belt profile, dead weight starts to free fall and rotates the shaft via the pulley. Then, after a predefined amount of time, Arduino sends the catch signal. As the solenoid is off OPS pushes the belt to the key profile and holds the weight. Throughout all the process, Arduino samples the encoder signal so that we can observe the amount of time until the weight is stable hold. A test case with a $40ms$ between the release-catch signals and a $1kg$ of dead-weight is shown in Figure 5.6.

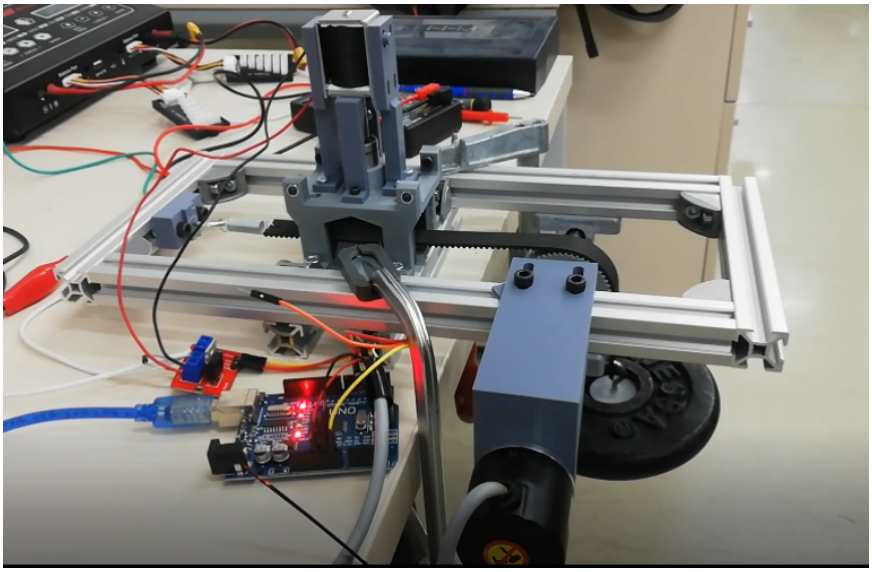

Figure 5.5: Test setup for conducting release/catch experiment for clutch

In conclusion, the bench-top test setup is able to lock an accelerated weight within $20 - 50ms$. And, we observe that holding capacity and speed of the clutch can be improved with changing design parameters like return spring force, matching tooth profile and number etc. Therefore, these preliminary results are accepted as the functionality of the proposed concept. More effort is spent on adapting this concept design on the existing hopper mechanism with a modular design.

5.2 Modular Design

In the existing hopping mechanism, one end of the parallel spring is fixed on the wrapping cam by using an aluminum clamp as shown in Figure 5.7. The idea of the modular design is to remove the clamp fixing the spring, and extending the steel cable carrying the parallel spring. The cable is then guided into the clutch mechanism that will fix it instead of the clamp. One can see the CAD model of the proposed modular design in Figure 5.8a and the manufactured prototype of it in Figure 5.8b. A sturdy base to be mounted on the body of the leg is designed and 3D printed with PLA material. A powerful solenoid actuator is provided from a local manufacturer. Solenoid has a stroke length of $5mm$ and provides holding force up to $15kg$. Again, OPS is utilized as the return spring. In order to benefit from the solenoid as much as

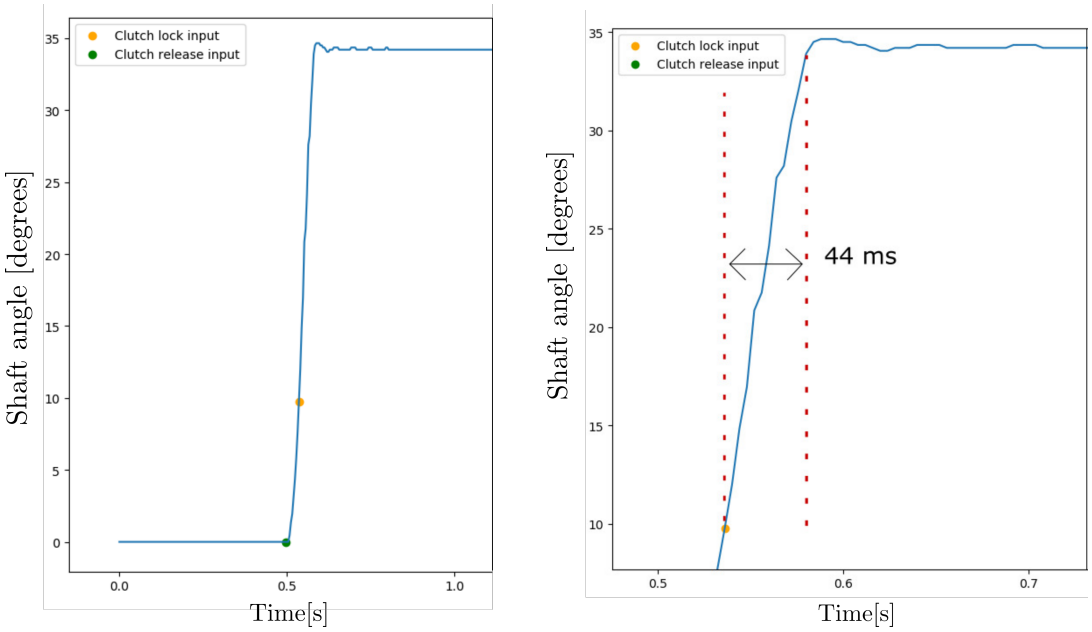

(a) Shaft angle vs time

(b) Catching time

Figure 5.6: Release/Catch Test for clutch

possible, wall thickness of the OPS is adjusted such that it provides a force close to the maximum of the solenoid when it elongates about $2mm$. 3M timing belt profile is used with a matching $3D$ printed tooth key to lock the spring. Two pulleys, mounted on the base with bearings, guide the spring cable without friction. Auxiliary spring is placed on the base to have a compact structure. In preliminary experiments, solenoid is able to release the spring without sticking with $1.5A$ current at $10V$ input voltage. The clutch is integrated on the leg as shown in Figure 5.9. Clutch is able to withstand forces created on the spring from the jumping trajectories introduced in Chapter 4 without slipping.

To assess the feasibility of this prototype mechanism in terms of energy efficiency, a case study is considered. By using the clutch mechanism, leg becomes able to shorten its length in the flight phase without opposing to the parallel spring. On the other hand, the clutch itself consumes some amount of energy to release the spring. In addition, the extra weight of the clutch would increase the required effort by the actuator to reach the same hopping heights. In hopping experiments of Chapter 4, system reaches apex heights of $0.3 - 0.35m$ and the flight phase lasts for approximately $0.2s$.

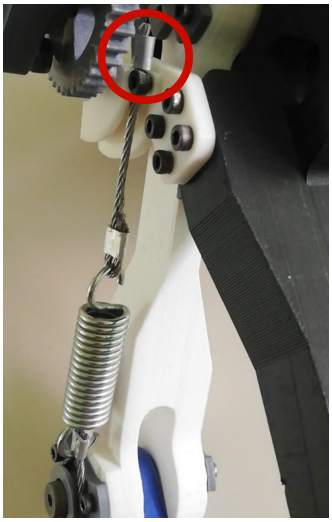

Figure 5.7: Fastening of the spring end in the original design. The fixing clamp is encircled.

We consider a case where the systems jump to an apex height of $0.34m$ and stays in air for $0.2s$. The open loop harmonic actuation input given in 4.1 with $0.3s$ actuation period is considered. The leg operates between $20° - 60°$ which corresponds to a leg height of $0.282m - 0.15m$. So, leg is able to shorten itself almost $13cm$ at most. Current geometric configuration of the clutch mechanism allows the auxiliary spring to elongate about $7cm$ that corresponds to $\approx 10cm$ contraction in leg length. A simple and smooth contraction trajectory for the leg in flight phase can be described as:

$$\delta z = Asin(\frac{2\pi t}{P}) \tag{5.1}$$

Where, A is the desired contraction amplitude, P is the period and δz refers to the contraction of the leg. To shorten the leg during the stance up to a certain height and re-contract it before the toe touches down, P can be chosen as $0.4s$. And, different amplitudes up to $10cm$ can be considered. Having this, symmetric contraction trajectory, work done against to the spring can be calculated as:

$$W = \frac{1}{2}\int_0^t \delta\dot{z}k(\delta z)dt$$

Half of the total integral is considered since the parallel spring opposes to the actuator only in the first half of the trajectory. With the given contraction trajectory, change of total energy consumption against the spring w.r.t different contraction amplitudes, A, is given in Figure 5.10a. Finding the change in the consume energy for reaching

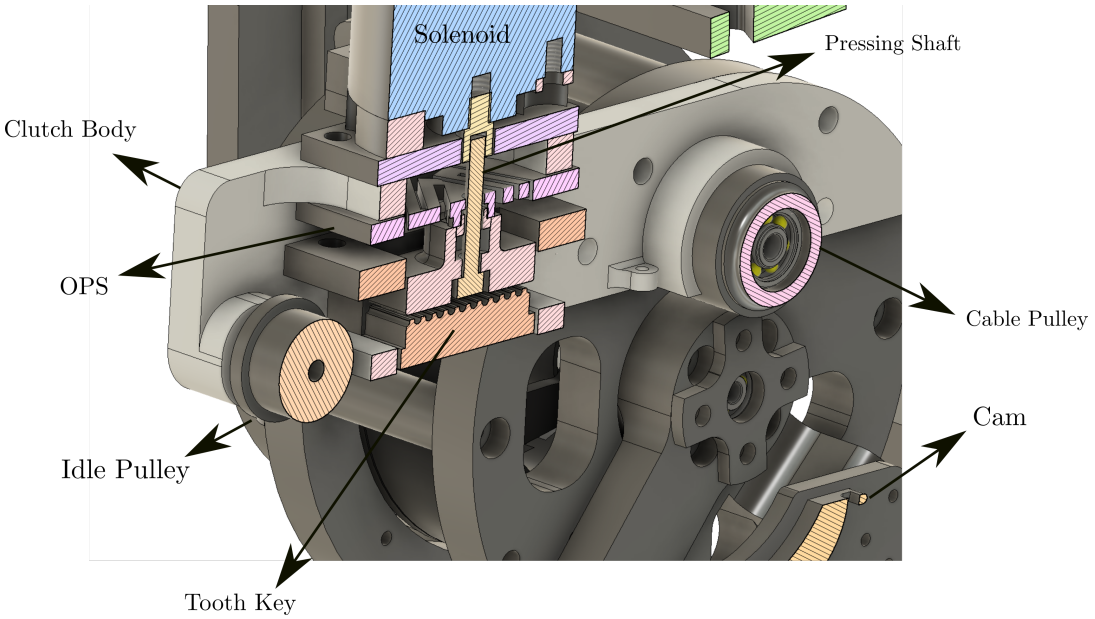

(a) CAD model showing the section view of the modular design

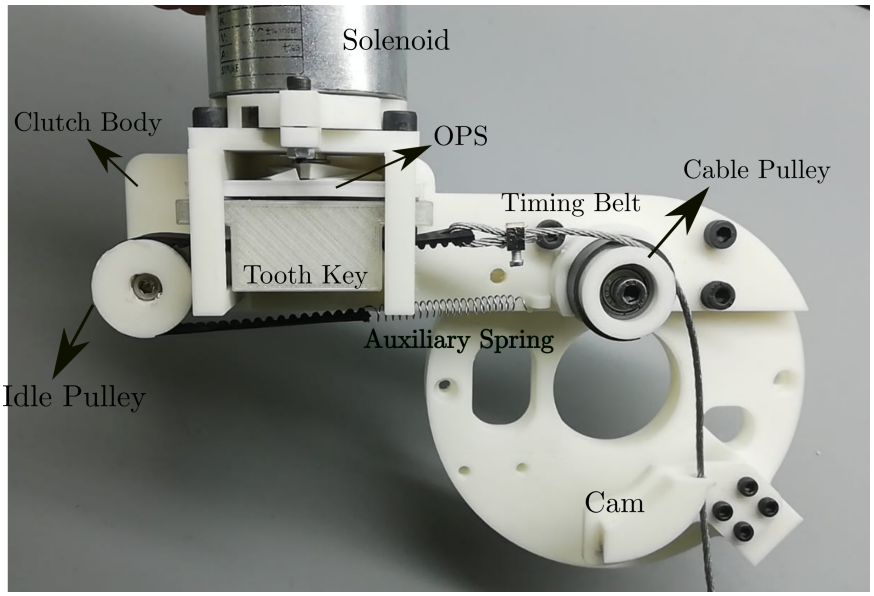

(b) Manufactured prototype of the modular design

Figure 5.8: Modular clutch design

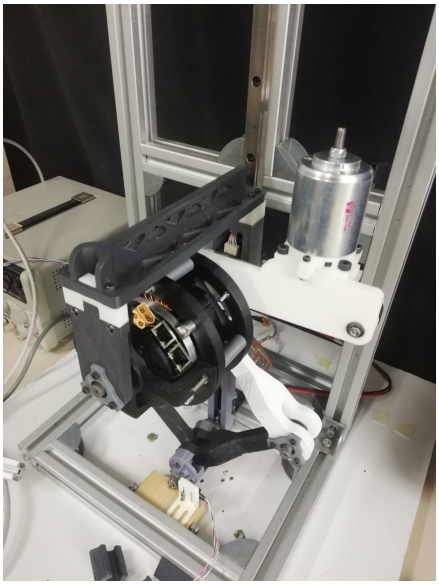

(a) Clutch mounted on the jumping test setup

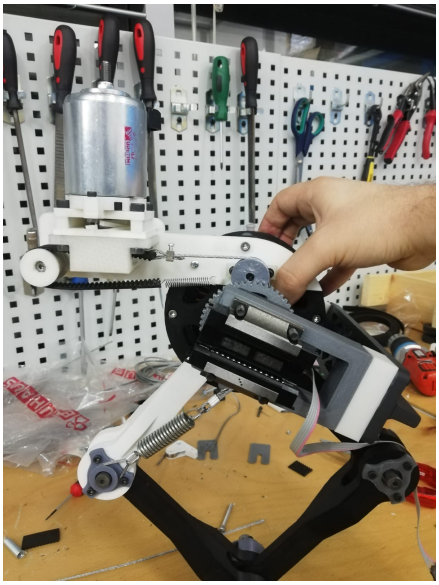

(b) Clutch mounted on the leg(back view)

Figure 5.9: Clutch mechanism mounted on the PEA hopper

the same height with the extra weight is not straightforward since equation of motion includes damping. Firstly, in order to find the actuation amplitude that results in the desired apex height MATLAB's $fzero$ method is used with different amplitude inputs. Then energy consumption is found by 5.1. Change of energy consumption with increasing mass of the clutch is given in the Figure 5.10b. Having a $700gr$ solenoid, total mass of the modular clutch mechanism is close to $1kg$. So, it increases consumption by $\approx 0.35J$. Finally, the energy consumed by the solenoid during the $0.2s$ flight phase is expected to be $\approx 3J$. For this simple case study, total energy consumption of the clutch seems to be on the same level of the negative effect of the parallel spring when the contraction length reaches up to $10cm$. However, the torque requirement for contracting the leg remains large as seen in the 5.11.

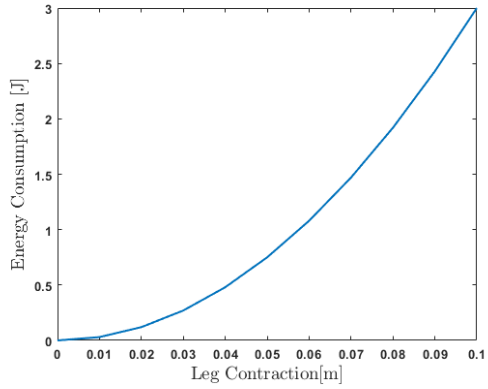

(a) Change of the energy consumption with increasing contraction length

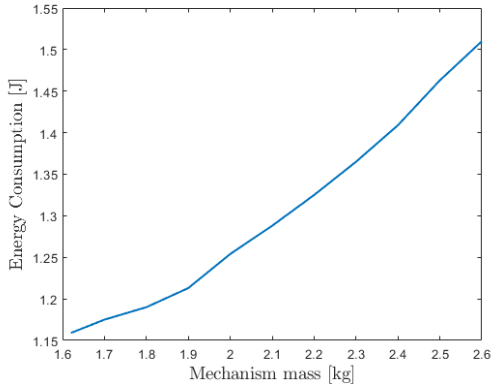

(b) Change of the energy consumption with increasing clutch mass

Figure 5.10: Change of the energy consumption

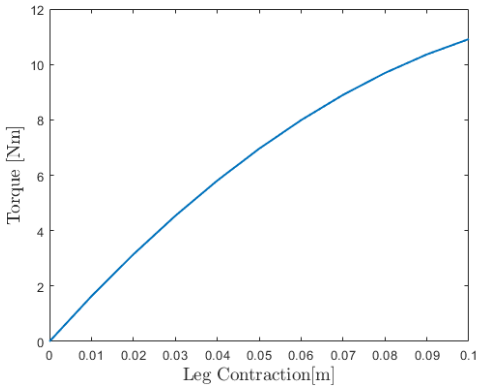

Figure 5.11: Change of the maximum required torque w.r.t contraction length

CHAPTER 6

DISCUSSION AND CONCLUSION

6.1 Discussion

6.1.1 Dynamical Models and Parameter Estimation

Parameter estimation of the stance and flight phases of the linear model is carried out using both the cumulative simulation error and the one-step prediction error methods. Although the simulation error method provided slightly better validation results in general, there is no distinctive difference between the two results. There seems to be a significant deviation between the damping coefficient of the stance phase, estimated by the two methods. However, a mass-spring-damper system is characterized by its damped natural frequency. Even the damping coefficients of the two methods differ, damped natural frequencies estimated by the two methods closely match each other. The spring coefficient is taken from measurement throughout the study, and the lumped body mass is estimated. We observed that when the lumped mass is taken from the measurement and the spring coefficient is estimated, or both are left free for estimation, different physical parameters are found; however, the damped natural frequency remains in the $19.3-19.9 rad/s$ range. Consistency of the estimated natural frequency distribution indicates the system's linear character.

The cost function used to estimate the optimum parameters is the normalized version of the mean square error. Normalized cost function enables the comparison of the performance of trajectories with different lengths. Also, it enables the consideration of both the position and velocity tracking performance simultaneously. For consistency, validation results are reported with the exact estimation cost. However, the interpre-

tation of the normalized mean square error is not straightforward. On the other hand, the mean average error directly reports the deviation of the predicted trajectory. Regardless of the time duration or the range of the motion, the main goal is to predict the correct position at the corresponding time. For the stance phase, estimated parameters resulted in an average of $2mm$ mean absolute error for 60 validation trajectories with 5 outliers. In any of them, the maximum deviation from the experimental position does not exceed $7mm$ at any time. High accuracy prediction performance and consistent natural frequency imply the validity of the linear mass-spring-damper model.

In general, measured COM velocity in the stance phase is much smoother than the measurements of the flight phase. We observe that this is due to the large mass and spring forces dominating the motion in the stance phase. Also, the prismatic joint of the toe constructed with a ball bearing and a rectangular slot results in sticking during the motion. Therefore, in general, the flight phase velocity has more noise. Efforts for estimating flight parameters showed that it is impossible to find a reasonable damping coefficient without proper filtering of the velocity. Because of the absence of active forces, initial conditions are decisive for accurately predicting the motion in the flight phase. As the velocity profile is noisy, estimation tends to converge to points. Even if a realistic parameter is found, the validation result is also affected by the noisy initial conditions. Therefore, filtered velocity profile is used to estimate and validate the flight phase. After proper filtering, 20 validation trajectories resulted in an average mean absolute error in position is less than $2mm$.

Both the touch-down and lift-off impacts result in a chaotic change in the COM velocity. Having estimated the stance and flight dynamics separately, impact parameters serve as a binder to transfer the states to correct initial conditions during the phase change. In that sense, optimizing impact parameters to get the most accurate motion is a platform-specific pragmatic solution. However, despite the inevitable time shift due to the contact switch, in overall, linear model is able to accurately predict the motion of the physical system.

The non-linear model is expected to be more accurate against the linearized model considering the less amount of simplifications. However, for the present physical platform, the inertial effects of the lower limbs turned out to be too small. Therefore,

the deviation of the estimated parameters a and b is relatively large. Despite the deviation, since these parameters have a minor contribution to the motion, validation results of the non-linear model are at the same level as the linear model. However, the model is observed to be sensitive to these parameters at the contact instant. A small change in the inertial parameters of the lower limbs causes chattering or a velocity jump in an unexpected direction. Nonetheless, the non-linear model promises a more generic equation of motion, which is expected to work well for the heavier legs systems and the generic planar motion.

6.1.2 Clutch Design

We have performed limited preliminary experiments to show the proposed clutch mechanism's functionality and feasibility. Although a relatively compact and reproducible design is achieved, actuator optimization seems to be the bottleneck of the design. The effect of the clutch's extra weight seems to be negligible against the electrical energy consumption due to the solenoid. Nevertheless, since the impact losses may increase with the added weight, one must choose a linear actuator that can provide the highest possible force compared to its mass and activation energy. The case study shows that the total energy consumption of the solenoid barely meets the negative work due to the parallel spring. However, the case study considers a limited swing leg trajectory. When the robot needs to make abrupt maneuvers, the effect of the clutch becomes prominent. Even the case study does not notice energy consumption improvement; maximum torque requirement rises up to $10Nm$ without a clutch. The thermal losses due to high torques must also be examined in further study. Moreover, the clutch may enable a smaller motor with lower torque capacity. Finally, a monopedal platform is considered in this study with an external controller PC and power unit. Typically, on-board power units, motor drivers, sensors and controller lead to a heavier overall structure. As the weight of the platform increases, we expect that the extra weight disadvantage of the clutch will become insignificant since its percentage will fall.

6.2 Conclusion

This study presents the modeling and experimental verification of a parallel elastically actuated hopping mechanism. While the previous study on this mechanism proves the energetic superiority of the parallel elasticity, we focus on the parameter estimation and the experimental performance of the platform. A data-driven parameter estimation method is adopted. First, the dynamical model is constructed, and the parameters are obtained to fit the experimental measurements to these models. Systematic cross-validation results evaluating the performance of these parameters show that the constructed physical model resembles a linear mass-spring-damper model as intended.

In addition to the experimental verification of the original system, we present a novel clutch mechanism design to increase the usability of the parallel elastic actuator. The mechanism has a compact design that is suitable for scaled platforms with 3D printed parts and off-the-shelf components. The crucial aspects of the design are, first, tested with a bench-top preliminary setup, and then a modular design to be integrated on the existing hopper platform is manufactured. A case study is provided to show that with the current product architecture, energetic efficiency is not expected to be improved on the existing platform; however, utilizing the clutch mechanism will be beneficial for reducing maximum torque requirements.

6.2.1 Future work

The results of the parameter estimation study clear the way for design and evaluation of new locomotion controllers. As we have the set of parameters that predicts the motion accurately, controllers optimized in the simulation environment are expected to work well in the physical setup. Time shift in the contact detection seems to be a limitation for the usage of the test setup. More advanced state estimation algorithms that do not depend on the external measurements can be employed to increase the reliability of the platform.

The apparent future work is to extend this monopedal test platform to a floating base mobile robot. Currently, motor of the platform is rigidly attached to one of the upper

links and rotates with it. In traditional leg structures we often see that stator of the motor is rigidly mounted on the body of the robot and both of the legs are assembled to the rotor of the motor with revolute joints. Updating the existing structure accordingly seems to be a better option. This structure is also more suitable for integrating the proposed clutch design. With a better selection of the solenoid actuator for the clutch, the next step is to perform release/catch experiments during the hopping cycle and evaluate the overall efficiency with real experimental measurements.

REFERENCES

[1] S. Ş. Candan, O. K. Karagöz, Y. Yazıcıoğlu, and U. Saranlı, "Design of a parallel elastic hopper with a wrapping cam mechanism and template based virtually tunable damping control," in *Dynamic Systems and Control Conference*, vol. 84270, p. V001T05A009, American Society of Mechanical Engineers, 2020.

[2] M. H. Raibert, *Legged robots that balance*. MIT press, 1986.

[3] P. Holmes, R. J. Full, D. Koditschek, and J. Guckenheimer, "The dynamics of legged locomotion: Models, analyses, and challenges," *SIAM review*, vol. 48, no. 2, pp. 207–304, 2006.

[4] I. Poulakakis and J. W. Grizzle, "The spring loaded inverted pendulum as the hybrid zero dynamics of an asymmetric hopper," *IEEE Transactions on Automatic Control*, vol. 54, no. 8, pp. 1779–1793, 2009.

[5] U. Saranlı, Ö. Arslan, M. M. Ankaralı, and Ö. Morgül, "Approximate analytic solutions to non-symmetric stance trajectories of the passive spring-loaded inverted pendulum with damping," *Nonlinear Dynamics*, vol. 62, no. 4, pp. 729–742, 2010.

[6] D. J. Hyun, S. Seok, J. Lee, and S. Kim, "High speed trot-running: Implementation of a hierarchical controller using proprioceptive impedance control on the mit cheetah," *The International Journal of Robotics Research*, vol. 33, no. 11, pp. 1417–1445, 2014.

[7] C. Semini, N. G. Tsagarakis, E. Guglielmino, M. Focchi, F. Cannella, and D. G. Caldwell, "Design of hyq–a hydraulically and electrically actuated quadruped robot," *Proceedings of the Institution of Mechanical Engineers, Part I: Journal of Systems and Control Engineering*, vol. 225, no. 6, pp. 831–849, 2011.

[8] A. Spröwitz, A. Tuleu, M. Vespignani, M. Ajallooeian, E. Badri, and A. J.

Ijspeert, "Towards dynamic trot gait locomotion: Design, control, and experiments with cheetah-cub, a compliant quadruped robot," *The International Journal of Robotics Research*, vol. 32, no. 8, pp. 932–950, 2013.

[9] W. Khalil and E. Dombre, *Modeling identification and control of robots*. CRC Press, 2002.

[10] M. Gautier, "Dynamic identification of robots with power model," in *Proceedings of international conference on robotics and automation*, vol. 3, pp. 1922–1927, IEEE, 1997.

[11] İ. Uyanık, Ö. Morgül, and U. Saranli, "Experimental validation of a feedforward predictor for the spring-loaded inverted pendulum template," *IEEE Transactions on robotics*, vol. 31, no. 1, pp. 208–216, 2015.

[12] A. Abate, R. L. Hatton, and J. Hurst, "Passive-dynamic leg design for agile robots," in *2015 IEEE international conference on robotics and automation (ICRA)*, pp. 4519–4524, IEEE, 2015.

[13] M. Hutter, C. D. Remy, M. A. Höpflinger, and R. Siegwart, "Slip running with an articulated robotic leg," in *2010 IEEE/RSJ International Conference on Intelligent Robots and Systems*, pp. 4934–4939, 2010.

[14] P. M. Wensing, A. Wang, S. Seok, D. Otten, J. Lang, and S. Kim, "Proprioceptive actuator design in the mit cheetah: Impact mitigation and high-bandwidth physical interaction for dynamic legged robots," *IEEE Transactions on Robotics*, vol. 33, no. 3, pp. 509–522, 2017.

[15] B. Katz, J. Di Carlo, and S. Kim, "Mini cheetah: A platform for pushing the limits of dynamic quadruped control," in *2019 international conference on robotics and automation (ICRA)*, pp. 6295–6301, IEEE, 2019.

[16] G. Kenneally, A. De, and D. E. Koditschek, "Design principles for a family of direct-drive legged robots," *IEEE Robotics and Automation Letters*, vol. 1, no. 2, pp. 900–907, 2016.

[17] N. Kau, A. Schultz, N. Ferrante, and P. Slade, "Stanford doggo: An open-source, quasi-direct-drive quadruped," in *2019 International conference on robotics and automation (ICRA)*, pp. 6309–6315, IEEE, 2019.

[18] F. Grimminger, A. Meduri, M. Khadiv, J. Viereck, M. Wüthrich, M. Naveau, V. Berenz, S. Heim, F. Widmaier, T. Flayols, *et al.*, "An open torque-controlled modular robot architecture for legged locomotion research," *IEEE Robotics and Automation Letters*, vol. 5, no. 2, pp. 3650–3657, 2020.

[19] M. Hutter, *StarlETH & Co.: design and control of legged robots with compliant actuation*. PhD thesis, ETH Zurich, 2013.

[20] M. Hutter, C. Gehring, D. Jud, A. Lauber, C. D. Bellicoso, V. Tsounis, J. Hwangbo, K. Bodie, P. Fankhauser, M. Bloesch, *et al.*, "Anymal-a highly mobile and dynamic quadrupedal robot," in *2016 IEEE/RSJ international conference on intelligent robots and systems (IROS)*, pp. 38–44, IEEE, 2016.

[21] C. Hubicki, J. Grimes, M. Jones, D. Renjewski, A. Spröwitz, A. Abate, and J. Hurst, "Atrias: Design and validation of a tether-free 3d-capable spring-mass bipedal robot," *The International Journal of Robotics Research*, vol. 35, no. 12, pp. 1497–1521, 2016.

[22] G. Secer and U. Saranli, "Control of planar spring–mass running through virtual tuning of radial leg damping," *IEEE Transactions on Robotics*, vol. 34, no. 5, pp. 1370–1383, 2018.

[23] Y. Yesilevskiy, Z. Gan, and C. David Remy, "Energy-optimal hopping in parallel and series elastic one-dimensional monopeds," *Journal of Mechanisms and Robotics*, vol. 10, no. 3, p. 031008, 2018.

[24] T. Yang, E. R. Westervelt, J. P. Schmiedeler, and R. A. Bockbrader, "Design and control of a planar bipedal robot ernie with parallel knee compliance," *Autonomous robots*, vol. 25, no. 4, pp. 317–330, 2008.

[25] P. Arm, R. Zenkl, P. Barton, L. Beglinger, A. Dietsche, L. Ferrazzini, E. Hampp, J. Hinder, C. Huber, D. Schaufelberger, F. Schmitt, B. Sun, B. Stolz, H. Kolvenbach, and M. Hutter, "Spacebok: A dynamic legged robot for space exploration," in *2019 International Conference on Robotics and Automation (ICRA)*, pp. 6288–6294, 2019.

[26] F. Nan, H. Kolvenbach, and M. Hutter, "A reconfigurable leg for walking robots," *IEEE Robotics and Automation Letters*, pp. 1–1, 2021.

[27] D. F. B. Haeufle, M. D. Taylor, S. Schmitt, and H. Geyer, "A clutched parallel elastic actuator concept: Towards energy efficient powered legs in prosthetics and robotics," in *2012 4th IEEE RAS EMBS International Conference on Biomedical Robotics and Biomechatronics (BioRob)*, pp. 1614–1619, 2012.

[28] S. Diller, C. Majidi, and S. H. Collins, "A lightweight, low-power electroadhesive clutch and spring for exoskeleton actuation," in *2016 IEEE International Conference on Robotics and Automation (ICRA)*, pp. 682–689, 2016.

[29] B. Penzlin, M. Enes Fincan, Y. Li, L. Ji, S. Leonhardt, and C. Ngo, "Design and analysis of a clutched parallel elastic actuator," in *Actuators*, vol. 8, p. 67, Multidisciplinary Digital Publishing Institute, 2019.

[30] X. Liu, A. Rossi, and I. Poulakakis, "Spear: A monopedal robot with switchable parallel elastic actuation," in *2015 IEEE/RSJ International Conference on Intelligent Robots and Systems (IROS)*, pp. 5142–5147, 2015.

[31] *Six Dimensional Compliance Analysis of Ortho-Planar Springs for a Continuum Manipulator*, vol. Volume 5A: 38th Mechanisms and Robotics Conference of *International Design Engineering Technical Conferences and Computers and Information in Engineering Conference*, 08 2014. V05AT08A036.